Role of Surface Enthalpy Fluxes in Idealized Simulations of Tropical Depression Spinup

VARUN S. MURTHY

Department of Geology and Geophysics, Yale University, New Haven, Connecticut

WILLIAM R. BOOS

Department of Earth and Planetary Science, University of California, Berkeley, and Climate and Ecosystem Sciences Division, Lawrence Berkeley National Laboratory, Berkeley, California

(Manuscript received 14 April 2017, in final form 16 February 2018)

ABSTRACT

An idealized, three-dimensional, cloud-system-resolving model is used to investigate the influence of surface enthalpy flux variations on tropical depression (TD) spinup, an early stage of tropical cyclogenesis in which the role of surface fluxes remains incompletely understood. A range of simulations supports the hypothesis that a negative radial gradient of surface enthalpy flux outside the storm center is necessary for TD spinup but can arise from multiple mechanisms. The negative radial gradient is typically created by the wind speed dependence of surface enthalpy fluxes, consistent with some previous theories for tropical cyclone intensification. However, when surface enthalpy fluxes are prescribed to be independent of wind speed, spinup still occurs, albeit more slowly, with the negative radial gradient of surface enthalpy flux maintained by an enhanced air–sea thermodynamic disequilibrium beneath the cold core of the incipient vortex. Surface enthalpy flux variations seem more important for intensification than initial conditions. For example, a vortex forms and intensifies even from a state of rest when the center of the domain is initialized to be nearly saturated with water vapor, but this intensification is modest in amplitude and transient, lasting less than 12 h, without interactive surface enthalpy flux. Sustained spinup on time scales longer than a day does not occur when surface enthalpy fluxes are horizontally homogeneous or constant, even when fixed at the high value of 200 W m^{-2}. In the ensemble of simulations presented here, the vortex intensification rate scales linearly with the storm-scale surface enthalpy flux anomaly relative to the undisturbed environment.

1. Introduction

Tropical cyclogenesis refers to the series of events leading to the formation of a tropical, warm-core, cyclonic vortex. Tropical depression (TD) spinup is an early phase of tropical cyclogenesis, which culminates in a region of high column relative humidity (CRH), a closed cyclonic circulation, and sustained surface wind speeds less than 17 m s^{-1}. While the various stages of tropical cyclone (TC) intensification have been studied extensively, the role of surface enthalpy fluxes in the early stage of TD spinup is less thoroughly explored.

Precipitating convection has long been associated with TC intensification (Palmen 1948). It is now widely accepted that storm-scale intensification of the azimuthal wind can be attributed to a radial circulation that converges vorticity, with precipitation falling in the upward branch of that radial circulation (Emanuel 2003; Montgomery and Smith 2017). This precipitating ascent occurs in an ensemble of convective updrafts within the TC, with those updrafts producing strong vortex stretching and thus generating intense cyclonic vorticity anomalies that merge to increase the storm-scale vorticity (Montgomery and Smith 2017, and references therein). These rotating updrafts often occur in deep convection (e.g., vortical hot towers; Hendricks et al. 2004), but low-level vortex stretching can also be produced by cumulus congestus (Wang 2014). Kilroy et al. (2017) showed that such convective vortices play a central role throughout the stages of TC intensification, including genesis.

The precipitating ascent that concentrates vorticity is supported during TC genesis by surface fluxes of enthalpy and by a moist midtroposphere within the storm.

Corresponding author: Varun S. Murthy, varun.murthy@yale.edu

DOI: 10.1175/JAS-D-17-0119.1

A negative radial gradient of CRH, a measure of midtropospheric moisture, was deemed necessary for TC genesis in early axisymmetric studies (Emanuel 1997; Frisius 2006) and seen in numerous field campaigns (e.g., Bister and Emanuel 1997) and high-resolution numerical simulations (e.g., Wang 2012). Dunkerton et al. (2009) proposed the marsupial pouch framework, in which the critical layer of a tropical wave is most conducive for TC genesis. While the pouch initially contains more moisture than its environment, further moistening occurs during TC genesis (Wang 2012). The moistening that occurs during TD spinup, which results in a mesoscale region of nearly saturated air, is critical for some theories of subsequent TC intensification (e.g., Emanuel 1989) and is one focus of this study.

While the importance of precipitating ascent for concentrating vorticity and the importance of tropospheric moistening for supporting deep convection are widely accepted (e.g., Montgomery and Smith 2017), the role of surface enthalpy fluxes in TD spinup continues to be debated. A prominent theory for TC intensification involves the increase of boundary layer equivalent potential temperature by surface sensible and latent heat fluxes and the subsequent increase of upper-tropospheric temperatures in the convecting atmosphere. In particular, a positive feedback between TC surface winds and surface enthalpy fluxes, termed wind-induced surface heat exchange (WISHE; Emanuel 1986; Rotunno and Emanuel 1987), has been examined extensively throughout the TC life cycle. In a theory for TD spinup, Raymond et al. (2007, hereafter R07) also proposed that wind-dependent surface enthalpy fluxes increase CRH, which causes an increase in the storm-scale precipitating ascent that converges low-level vorticity. In contrast, Molinari et al. (2004) found that the boundary layer equivalent potential temperature was radially uniform during TD spinup, suggesting that it is a pre-WISHE stage, and Tang (2017) found that surface fluxes during early TC genesis increased moist entropy in the outer region of the storm more than the inner region. Whether the feedback between surface winds and surface fluxes is necessary for the intensification of weak, elevated vortices with a large saturation deficit (i.e., TD spinup) is thus an open question.[1]

The necessity of a wind–evaporation feedback (e.g., WISHE) for TC intensification in general—not just for the TD spinup phase—is also actively debated. Montgomery et al. (2009, 2015) showed that TC intensification was mostly unaffected when surface enthalpy fluxes were "capped" (i.e., constrained to be smaller than an imposed maximum), suggesting that the concurrent intensification of surface winds and surface fluxes in models and observations may be incidental. However, Zhang and Emanuel (2016) showed that WISHE was essential for the successful numerical simulation of at least one observed TC (Hurricane Edouard, 2014) and that intensification is inhibited when the surface fluxes are capped. Arguments against the necessity of WISHE for TC intensification acknowledge that surface evaporation increases as the TC circulation increases in strength, but note that intensification does not require this evaporation to continually increase with surface wind speed (Montgomery et al. 2009, 2015; Kilroy et al. 2016). This raises the question of whether the wind dependence of surface evaporation is necessary for TD spinup even if further intensification past the TD stage can proceed, albeit more slowly, without WISHE. For example, Kilroy et al. (2016, p. 2254) studied the observed spinup of one tropical low pressure system and noted that "enhanced surface moisture fluxes near the circulation centre play an important role in elevating moist equivalent potential temperature in the boundary layer, thereby supporting deep convection and, in turn, the intensification process." A seemingly contrasting summary is found in Montgomery et al. (2015, p. 92), who stated that for TC intensification to occur, "some minimal enthalpy fluxes are only needed to maintain convection." Examining the necessity of surface enthalpy flux variations for the spinup of weak tropical vortices is the main goal of this study. To be clear, these variations in surface enthalpy fluxes are often called a "feedback" because they involve two-way coupling with the storm state; any increase in surface enthalpy flux must necessarily be accompanied by vorticity concentration in precipitating ascent for TD spinup to constitute a feedback.

Surface flux feedback involving the air–sea enthalpy disequilibrium has received far less attention than that involving surface winds. Yet TDs are often characterized by peak midlevel vorticity in balance with a lower-tropospheric cold core (e.g., Yanai 1961; Raymond 2012), although this might be scale dependent (Wang 2012). This cold core has been hypothesized to increase surface enthalpy fluxes because of its enhanced air–sea thermodynamic disequilibrium (Tory and Frank 2010; Davis and Ahijevych 2013). However, in a study of the spontaneous TC genesis that occurs after moist convection self-aggregates in a cloud-system-resolving model, Wing et al. (2016) found that the air–sea disequilibrium provides a negative feedback on intensification. There is

[1] The term WISHE has traditionally been used in association with a mechanism in which surface fluxes enhanced by surface winds rapidly (within a few hours) cause convective heating near the vortex center. Since deep convective heating may not occur while the core of a subsaturated TD undergoes moistening, the positive feedback between surface winds and surface fluxes is not termed WISHE here, consistent with Raymond et al. (2007).

thus no clear agreement about the role of air–sea enthalpy disequilibrium during TD spinup.

How important is surface evaporation in moistening the TD vortex? Emanuel (1997) suggested that ocean surface evaporation moistens the atmosphere when CRH is low, with convective heating occurring only after the column is nearly saturated. In an axisymmetric model, Frisius (2006) found that surface evaporation enhanced by surface wind is required for maintaining a region with high CRH. While these studies suggest that surface evaporation increases the CRH of incipient TDs, causation is difficult to assess because local surface evaporation is typically small compared to the horizontal convergence of water vapor by the secondary circulation (e.g., Fritz and Wang 2014).

The main goal of this paper is to examine the role of surface enthalpy variations during TD spinup, with emphasis on variations driven by surface winds and air–sea enthalpy disequilibrium. Idealized cloud-system-resolving simulations of intensifying vortices are conducted in the absence of mean vertical wind shear, using an ensemble of initial conditions and modifications of surface fluxes. While vertical wind shear and baroclinic influences might be important for aspects of TD spinup (e.g., Nolan and McGauley 2012; Davis and Bosart 2003), this study explores the idealized scenario of intensification in a barotropic base state that has been used in many prior TC studies (e.g., Rotunno and Emanuel 1987; Montgomery et al. 2009).

Since the dynamic processes responsible for TD spinup, including vorticity convergence by rotating convection, have been studied in depth elsewhere (e.g., Montgomery and Smith 2017), the emphasis here is on the influence of surface enthalpy fluxes on storm evolution. Specifically, this paper examines the hypothesis that enhanced surface enthalpy fluxes near the center of the storm are required to maintain the precipitating ascent that produces vorticity convergence during the early stage of TD spinup.

The next section describes the numerical model and its configuration, and section 3 details relevant metrics. Section 4 elucidates the role of surface flux variations during spinup, and section 5 quantifies the relation between intensification rates and enthalpy flux variations. The paper concludes with a summary and discussion of the results.

2. Simulation design

a. Model details

Simulations are performed using version 6.3 of the System for Atmospheric Modeling (SAM; Khairoutdinov and Randall 2003), a three-dimensional, Cartesian-coordinate atmospheric model that solves prognostic equations for winds, liquid water and ice moist static energy, total nonprecipitating water, and total precipitating water using the anelastic approximation. We use a single-moment, five-species microphysics scheme that represents the evolution of cloud water, cloud ice, rain, graupel, and snow. A Smagorinsky-type closure is used to represent subgrid-scale turbulence. The lower boundary is an oceanic surface with fixed sea surface temperature (SST) of 301 K. The surface sensible heat flux (SHF) and latent heat flux (LHF) are parameterized using bulk formulas:

$$\begin{aligned} \mathrm{LHF} &= \rho_0 C_E L_v U (q^*_{\mathrm{SST}} - q_v), \\ \mathrm{SHF} &= \rho_0 C_H c_p U (\mathrm{SST} - T_a), \end{aligned} \tag{1}$$

where U, q_v, and T_a are, respectively, the wind speed, water vapor mixing ratio, and absolute temperature at the lowest model level; q^*_{SST} is the saturation water vapor mixing ratio at the SST and surface pressure; L_v is the latent heat of vaporization; and c_p is the specific heat of air at constant pressure. The density at the lowest model level ρ_0 is the same value used in the anelastic equations and has no spatial or temporal variations. The bulk exchange coefficients for latent and sensible heat, C_E and C_H, respectively, are fixed at 1.1×10^{-3}. A minimum value of $1\,\mathrm{m\,s^{-1}}$ is imposed on U to crudely account for subgrid-scale variability of surface winds. The simulations are performed on an f plane with the Coriolis parameter $f = 5 \times 10^{-5}\,\mathrm{s^{-1}}$. Parameterizations from the National Center for Atmospheric Research (NCAR) Community Climate Model, version 3 (CCM3; Kiehl et al. 1998) are used to represent longwave and shortwave radiation. Insolation is fixed at a perpetual value of $409\,\mathrm{W\,m^{-2}}$, with no diurnal or seasonal cycle.

All simulations use a $1024 \times 1024 \times 64$ grid, with a horizontal resolution of 2 km and doubly periodic lateral boundaries. The lowest model level is at 37 m, and the vertical resolution is roughly 250 m below 2 km and 400 m in the rest of the troposphere. The upper boundary is a rigid lid at 27 km and Newtonian damping is applied in the upper third of the domain to prevent gravity wave reflection. The model uses adaptive time stepping, with a maximum time step of 5 s and automatic halving to retain numerical stability.

b. Initial conditions

All numerical simulations are initialized with horizontally homogeneous temperature and water vapor mixing ratio profiles and no background wind. The temperature and moisture profiles are the horizontal average of the final 25 days of a 100-day simulation integrated over a smaller domain ($80 \times 80 \times 64$ grid points) with the same horizontal resolution and boundary conditions. Such initial conditions have previously

been used to study tropical cyclogenesis starting from radiative–convective equilibrium (RCE; e.g., Nolan et al. 2007). The relative humidity (RH) is greater than 90% both in the lower troposphere (0–2-km altitude) and at the tropopause (13–14-km altitude), consistent with the "C" shape of the time-mean tropical RH (e.g., Romps 2014). With a surface temperature of 301 K, the initial sounding has surface-based, pseudoadiabatic convective available potential energy (CAPE) of 1200 J kg^{-1}.

c. Structure of the seed vortex

A weak, balanced, axisymmetric vortex, characterized by a tangential wind field $V(r, z)$, is introduced in the center of the domain. The vortex is in gradient wind balance with an axisymmetric temperature perturbation $T'(r, z)$, which is tapered to zero at a radius r of 500 km (detailed equations specifying T' and V are given in the appendix). In a majority of our simulations, including the control (Mid5; see Table 1), a midlevel vortex in balance with a warm-over-cold temperature structure (Fig. 1a) is used as an idealization of TC precursors (e.g., Raymond et al. 1998). The temperature perturbation is tuned to obtain maximum winds of 5 m s^{-1} at 3-km altitude and about 150-km radius, surface wind speed that is one-quarter the maximum wind speed at 3 km, and winds that taper to zero at 10 km. Some simulations are instead initialized with a vortex having peak winds at the surface, with T' positive throughout the troposphere.

The temperature anomaly associated with the axisymmetric vortex modifies the RH of the otherwise horizontally homogeneous initial state. For a midlevel vortex, this increases RH in the lower troposphere and decreases it in the upper troposphere (Fig. 1b, shading).

Additional simulations are initialized with a positive moisture anomaly in the center of the domain. The moisture anomaly is introduced as an axisymmetric RH perturbation RH$'(r, z)$, with a maximum value of 30% at an altitude of 6 km (Fig. 1b, contours). The formulation of RH$'$ is presented in the appendix.

d. List of simulations

The idealized simulations are divided into seven groups (Table 1), each designed to examine a specific aspect of surface flux feedback during TD spinup. The first part of the name given to each simulation indicates the altitude and intensity of the vortex. In most simulations, a midlevel vortex with peak wind speed of 5 m s^{-1} at 3-km altitude is used, indicated by the prefix "Mid5." The prefix "Sfc" indicates a vortex with peak winds at the surface, in which case the initial vertically averaged circulation is set equal to that in the control. The prefix "V0" is used when no initial vortex is used (i.e., the initial condition is a state of rest).

Subsequent parts of the names given to each simulation denote properties of the initial condition (groups B and G) or modifications to the bulk flux formulas for sensible and latent heat (groups C–F). Section 4 discusses results from these simulations, along with their design and objectives.

3. Analysis methods

a. Metric for TD spinup

The National Oceanic and Atmospheric Administration's National Hurricane Center (NOAA/NHC) defines a TD as a cyclonic vortex with peak surface winds not exceeding 17 m s^{-1}. Since this definition lacks a lower wind speed threshold, we seek a metric that could be used to define TD spinup.

The importance of an appropriate metric is illustrated by three of our simulations: the control (Mid5), a simulation in which surface wind speeds in the surface flux parameterization are limited to 5 m s^{-1} (Mid5_Cap5), and a simulation in which surface enthalpy fluxes are eliminated entirely (Mid5_FlxOFF). Results from these simulations are discussed in detail in the next section, with select time series shown here to illustrate the importance of an appropriate spinup metric. In these simulations, inspection of the three-dimensional wind field shows that the vortex in Mid5 intensifies the fastest and transitions into a warm-core vortex on day 3. In contrast, Mid5_FlxOFF exhibits no vortex intensification, and the vortex in Mid5_Cap5 intensifies more slowly than in the control and transitions into a warm-core vortex on day 4 (not shown). However, peak surface wind speeds in all three simulations are very similar from day 1.0 through day 2.5 (Fig. 2a). The threshold of 8.5 m s^{-1} marked in Fig. 2a is used by the India Meteorological Department to classify synoptic-scale vortices as monsoon depressions (Saha et al. 1981); many of the dynamical structures and genesis statistics of monsoon depressions are similar to those of TCs (Cohen and Boos 2016; Ditchek et al. 2016). All three of our vortices exceed the 8.5 m s^{-1} threshold, even though the Mid5_FlxOFF vortex does not intensify. This seems to be due to convective gustiness, showing that the peak surface wind speed is a poor measure of TD spinup.

The maximum speed of the azimuthal-mean tangential surface wind enables a clearer distinction between intensifying and nonintensifying vortices (Fig. 2b). However, ambiguity about the degree of intensification persists during the first 2–2.5 days of the simulations.

An appropriate metric should capture changes in elevated winds to account for intensification of a midlevel

TABLE 1. List of idealized simulations.

Group	Name	Description
Group A: Control simulation	Mid5	Initial vortex has peak winds of 5 m s^{-1} at an altitude of 3 km. Surface fluxes are a function of surface wind speed and air–sea enthalpy disequilibrium.
Group B: Initial-condition ensemble	Mid5_CAPEx1.5	Initial CAPE is increased by a factor of 1.5 everywhere in the domain by applying a Gaussian-shaped, negative temperature anomaly (peak amplitude = −3 K) to the temperature sounding between 1- and 15-km altitude.
	Mid5_RH85	Initial RH is set to 85% from the surface to 15-km everywhere in the domain.
	Sfc5	Initial vortex has peak winds of 5 m s^{-1} at the surface. The initial vertically averaged circulation of the vortex in this simulation is equal to the control.
Group C: Surface fluxes driven purely by air–sea enthalpy disequilibrium	Mid5_Fix10	Surface wind is fixed at 10 m s^{-1} when computing surface enthalpy fluxes.
	Sfc5_Fix10	Initial vortex has peak winds of 5 m s^{-1} at the surface and surface wind is fixed at 10 m s^{-1} when computing surface enthalpy fluxes.
	Mid5_Fix5	Surface wind is fixed at 5 m s^{-1} when computing surface enthalpy fluxes.
Group D: Horizontally homogeneous surface enthalpy fluxes	Mid5_FlxOFF	Surface enthalpy fluxes are switched off.
	Mid5_FlxHOM	Surface enthalpy fluxes are horizontally homogenized at each model time step.
	Mid5_LHF200	Surface evaporation is fixed at 200 W m^{-2} and sensible heat flux is switched off.
Group E: Horizontally homogeneous surface evaporation	Mid5_LHF0	Surface evaporation is switched off and sensible heat flux is interactive.
	Mid5_LHF0_SHFx5	Surface evaporation is switched off and the sensible heat flux is increased by a factor of 5.
Group F: Surface winds capped in the surface enthalpy flux parameterization	Mid5_Cap2	Surface wind is capped at 2 m s^{-1} when computing surface enthalpy fluxes.
	Mid5_Cap5	Surface wind is capped at 5 m s^{-1} when computing surface enthalpy fluxes.
Group G: Simulations initialized with a moist anomaly	Mid5_Moist	In addition to a midlevel vortex with peak winds of 5 m s^{-1}, the domain is initialized with a moist anomaly.
	Mid5_Moist_FlxOFF	As in Mid5_Moist, but surface fluxes are switched off.
	V0_Moist	Domain is initialized only with a moist anomaly; initial tangential winds are set to 0 m s^{-1}.
	V0_Moist_FlxOFF	As in V0_Moist, but surface fluxes are switched off.
	V0_Moist_LHF200	As in V0_Moist, but surface evaporation is fixed at 200 W m^{-2}.
Miscellaneous simulations	Mid5_ΔTΔqHOM	Temperature and moisture disequilibria (ΔT and Δq, respectively) are horizontally homogenized at each model time step prior to the computation of surface fluxes.

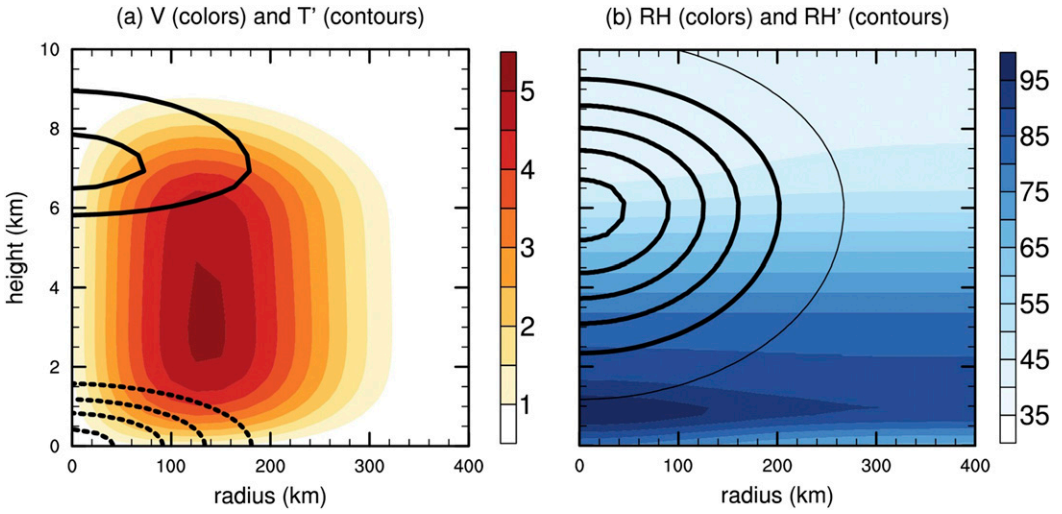

FIG. 1. (a) Axisymmetric tangential wind (colors) and axisymmetric temperature anomaly (contours; interval of 0.5 K, and negative values are dashed) of the initial vortex in the control (Mid5; midlevel vortex with peak winds of 5 m s^{-1}) simulation. The temperature anomaly is with respect to the initial domain-mean temperature. (b) Azimuthal-average RH of the initial state (colors) in the control (Mid5) simulation. RH of the moisture perturbation used in the group G (see Table 1) simulations is shown by contours (interval of 5%; thin contour depicts zero perturbation).

vortex that might not manifest at the surface. Here, we use the circulation vertically averaged between the surface and 10 km:

$$\Gamma = \left\langle \iint (f + \hat{\mathbf{k}} \cdot \nabla \times \mathbf{u})\, dx\, dy \right\rangle, \qquad (2)$$

where $\mathbf{u}$ is the horizontal velocity, the angle brackets denote mass-weighted vertical averages between the surface and 10 km, and the area integral is calculated over a 500-km square centered on the surface pressure minimum. The time evolution of this vertically averaged circulation clearly depicts differences in the intensification of the three vortices (Fig. 2c). Marín et al. (2008) used a similar metric, albeit with different horizontal and vertical extent, to depict TC intensification. Here, thresholds of 18 and 25 km^2 s^{-1}, respectively, are used to define the bounds between which a TD exists and are determined empirically. A warm-core vortex formed in a wide range of our simulations for $\Gamma > 25$ km^2 s^{-1},

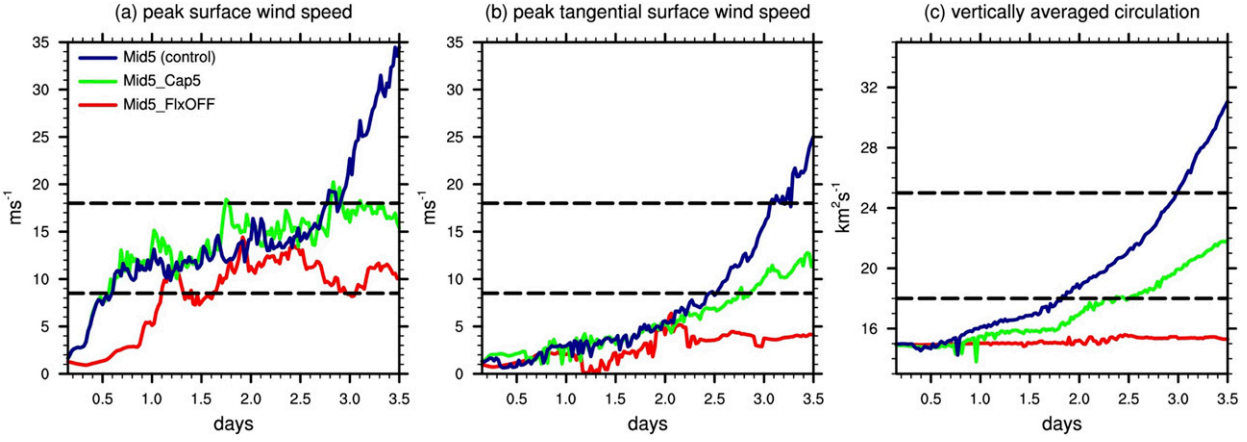

FIG. 2. Time evolution of (a) peak surface wind speed, (b) storm-centered, peak azimuthal-mean tangential surface wind, and (c) storm-centered, 0–10-km vertically averaged circulation in the control simulation (Mid5), simulation with surface wind capped at 5 m s^{-1} in the surface flux parameterization (Mid5_Cap5), and simulation with surface fluxes switched off (Mid5_FlxOFF). The average circulation is obtained by integrating the absolute vorticity in a 500-km square around the storm center and subsequently averaging between 0 and 10 km. Dotted lines depict the lower and upper thresholds of wind speed and circulation used to identify tropical depressions.

signaling the end of TD spinup. A value of $\Gamma = 18\,\mathrm{km^2\,s^{-1}}$ typically coincided with peak midlevel tangential winds of $8.5\,\mathrm{m\,s^{-1}}$, average CRH values beyond 80%, and a prominent increase in precipitation rates. These thresholds vary with the horizontal extent of integration and the depth of vertical averaging. Furthermore, the vertically averaged circulation is sensitive to the size of the vortex and can only be used to compare the intensification of similarly sized vortices, like those in the idealized simulations of this study.

b. Decomposition of surface fluxes

To estimate the individual contributions of surface wind speeds and air–sea thermodynamic disequilibrium to TD spinup, the total surface enthalpy flux is decomposed into wind-driven and disequilibrium-driven components. Following Wing and Emanuel (2014), we linearize Eq. (1) about the domain-mean state:

$$\begin{aligned} \mathrm{SF}' = {} & \rho_0 U'(C_E L_v \overline{\Delta q} + C_H c_p \overline{\Delta T}) \\ & + \rho_0 C_E L_v \overline{U} \Delta q' + \rho_0 C_H c_p \overline{U} \Delta T', \end{aligned} \tag{3}$$

where overbars and primes denote, respectively, horizontal domain-mean quantities and corresponding spatial anomalies. The three main terms on the right-hand side of Eq. (3) are the wind, moisture disequilibrium ($\Delta q = q^*_{\mathrm{SST}} - q_v$), and temperature disequilibrium ($\Delta T = \mathrm{SST} - T_a$)-driven anomalies, respectively. Flux anomalies due to the product of anomalies of surface wind and thermodynamic disequilibrium are extremely small in our simulations. Furthermore, density anomalies do not appear in Eq. (3) owing to constant density in Eq. (1), consistent with the anelastic approximation.

4. Results

a. Surface fluxes in the control simulation

We begin by diagnostically examining variations in surface enthalpy fluxes during TD spinup in the control simulation, Mid5. Since our primary interest is the role of surface flux feedback, we only briefly discuss the overall dynamics of spinup, noting similarities with details discussed in previous studies (Montgomery and Smith 2017, and references therein).

Intensification and moistening of the midlevel vortex, here referred to as TD spinup, last until the formation of a warm-core vortex on day 3. During the initial stages of spinup, the peak vertical mass flux occurs at approximately 7.5-km altitude (not shown). Later stages of spinup are associated with heavier precipitation rates and a lowering of the height of the peak vertical mass flux, consistent with previous observations (Raymond and Carrillo 2011). The vertical mass flux is associated with a radial secondary circulation hypothesized to converge vorticity. Indeed, the observed Eulerian time tendency of absolute vorticity during spinup is approximately in balance with horizontal vorticity convergence (not shown), consistent with Wang (2012).

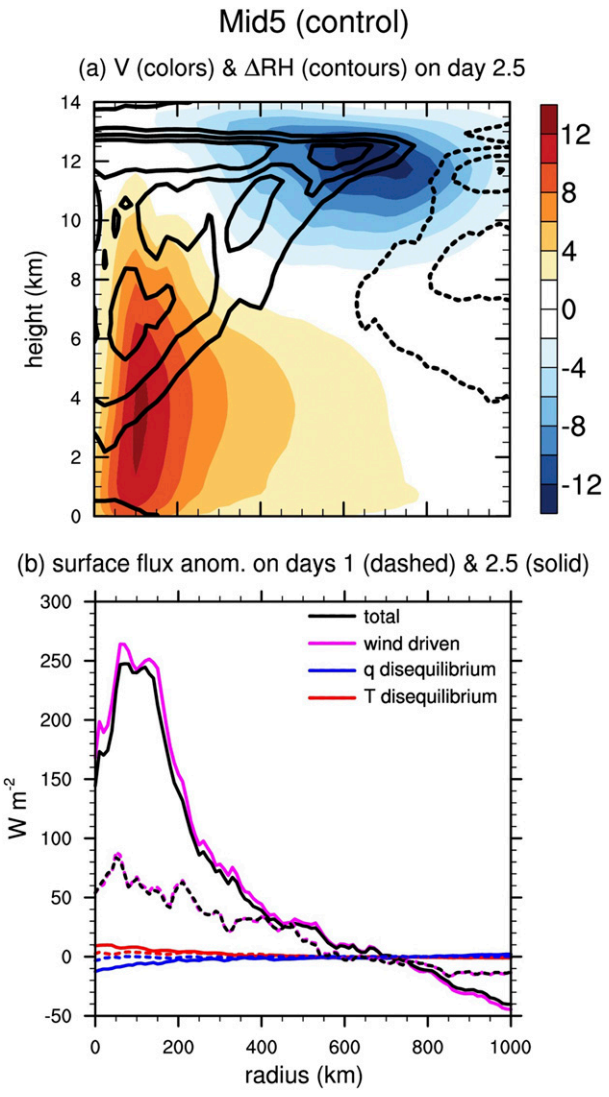

FIG. 3. (a) Azimuthal-average tangential winds (colors) and increase in RH (contours; interval of 10%, negative values are dashed) on day 2.5 in the control (Mid5) simulation. The increase in RH is with respect to the initial moisture shown by shading in Fig. 1b. (b) Decomposition of surface flux anomalies on day 1 (dashed) and day 2.5 (solid) in the control (Mid5) simulation. The surface flux anomalies are computed with respect to the domain-mean surface flux.

On day 2.5, peak tangential winds occur at 3.5-km altitude and 100-km radius (Fig. 3a, shading). The midlevel vortex is associated with negative temperature anomalies (peak value λ −3 K) below 3 km and positive

anomalies (peak value $\simeq 2$ K) above 4 km (not shown). RH increases by up to 30% compared to the initial condition, leading to values exceeding 90% (Fig. 3a, contours). High CRH has been suggested to foster large precipitation rates by reducing entrainment of dry air and supporting strong convective updrafts (see section 1). The negative radial gradient of CRH makes the vortex, and not its environment, conducive for deep moist convection. Further details of vortex moistening are discussed in section 4e.

It has been hypothesized that the early stages of TC genesis could be strongly influenced by interactions between radiation, water vapor, and clouds (Khairoutdinov and Emanuel 2013; Wing et al. 2016). Yet in additional simulations not listed in Table 1, TD spinup occurs when radiative temperature tendencies are horizontally homogenized at each model time step but is suppressed when the homogenization is applied to surface enthalpy fluxes. Concluding that radiative feedback is not essential for TD spinup in our idealized simulations, we focus purely on surface flux feedback, and interactions with radiation are not discussed further.

Positive surface flux anomalies occur within the vortex during TD spinup, with peak values increasing from about 80 to 250 W m^{-2} between day 1 and day 2.5 (Fig. 3b, black curve), consistent with the simulations of Montgomery et al. (2009). The positive and negative areas under the curves in Fig. 3b are not identical owing to the exclusion of parts of the domain (e.g., corners) during azimuthal averaging. The negative radial gradient of surface fluxes is almost entirely due to wind enhancement of surface fluxes (Fig. 3b, magenta curves).[2] The correlation between surface wind speed and wind-driven surface fluxes by itself does not imply a feedback process; results from simulations in which the influence of surface winds on surface fluxes is curtailed are discussed in section 4f.

The intensifying TD is associated with enhanced values of near-surface water vapor mixing ratio within the vortex and with negative temperature anomalies below the altitude of maximum winds, even within the boundary layer (not shown). The effect of these near-surface moisture and temperature changes on the pattern of surface enthalpy fluxes via air–sea enthalpy disequilibrium is now examined. The enhanced near-surface moisture suppresses the disequilibrium-driven surface evaporation by roughly 10 W m^{-2} on day 2.5, but the cold core enhances disequilibrium-driven sensible heat fluxes by a similar small amount (Fig. 3b, blue and red curves). The influence of disequilibrium-driven surface fluxes on spinup is examined in Mid5_ΔTΔqHOM, a simulation in which the temperature and moisture disequilibria (ΔT and Δq, respectively) are horizontally homogenized at each model time step prior to the computation of surface fluxes. TD spinup proceeds almost identically as in the control simulation (Fig. 4a, magenta curve), confirming the negligible role of disequilibrium-driven compared to wind-driven surface flux feedback.

b. *Sensitivity to initial conditions*

We now test the sensitivity of spinup in our control simulation to perturbations in initial conditions. Rather than using a large ensemble with randomly perturbed initial states, we use a three-member ensemble with large variations in initial CAPE, moisture, and initial vortex structure (Table 1, group B). In particular, one ensemble member starts from a state in which CAPE was increased by a factor of 1.5 by applying a Gaussian shaped, negative temperature anomaly (peak amplitude = −3 K) to the initial temperature sounding between 1 km and 15 km altitude. In another ensemble member, the initial humidity was increased to achieve an RH of 85% everywhere below 15-km altitude. A third ensemble member used an initial vortex having peak winds at the surface, but the same vertically averaged circulation as the control simulation. To be clear, we do not intend to perform an exhaustive study of the sensitivity of TD spinup to initial conditions but to provide some confirmation of the robustness of our conclusions about the role of surface flux feedback.

Enhanced CAPE does not accelerate TD spinup (Mid5_CAPEx1.5; Fig. 4a, red curve), consistent with simulations presented by Montgomery et al. (2009). This is presumably because moist convection consumes CAPE and restores the temperature profile to a moist adiabat faster than the roughly 3-day time scale associated with TD spinup. When initialized with 85% RH, TD spinup is accelerated (Mid5_RH85; Fig. 4a, blue curve), consistent with the hypothesis that tropospheric moistening is an important part of TD spinup (Nolan 2007). When the initial condition uses a surface vortex rather than a midlevel vortex, the rate of TD spinup increases, with rapid intensification during the first 20 h (Sfc5; Fig. 4a, green curve). In that simulation, strong surface winds enhance surface enthalpy fluxes and lead to the convergence of vorticity by precipitating convection. After 20 h, low-level divergence transforms the surface vortex into a midlevel vortex similar to that used in the initial condition of the control simulation. The formation of a midlevel vortex

[2] The term negative radial gradient is used here to describe the enhancement of surface fluxes in the inner parts of the vortex relative to the undisturbed environment. A positive radial gradient of surface fluxes typically exists between the vortex center (zero radius) and the radius of maximum wind, but we refer only to the negative radial gradient that exists between the radius of maximum wind and larger radii, consistent with prior studies (e.g., Emanuel 1997; Montgomery et al. 2009).

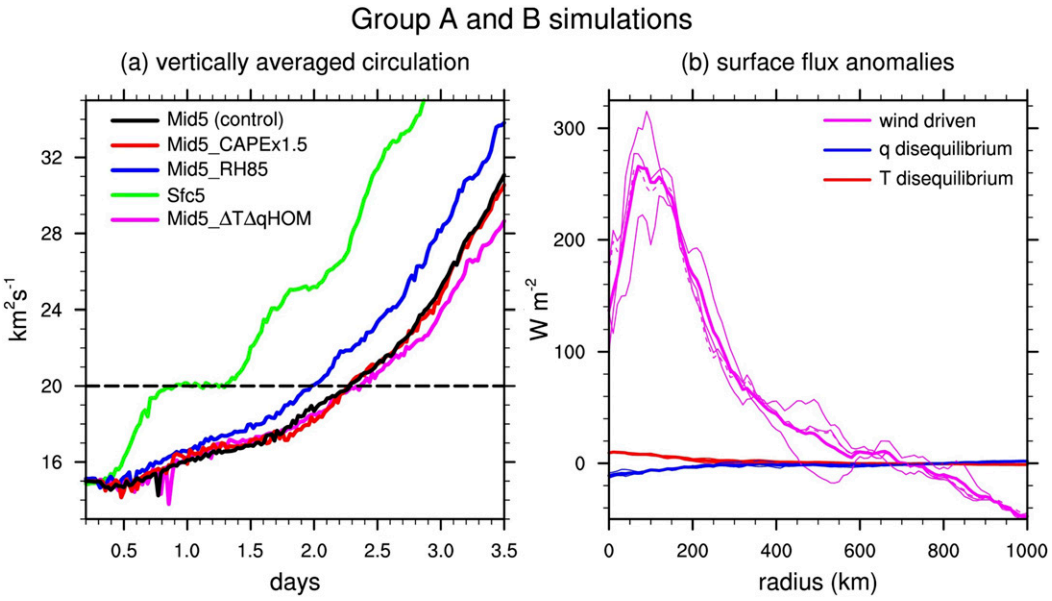

FIG. 4. (a) Time evolution of the 0–10-km vertically integrated circulation in a 500-km box tracking the vortex and (b) decomposed surface flux anomalies in the individual group B ensemble of simulations (thin solid curves) and the ensemble mean (thick solid curves). Surface flux anomalies in the ensemble members are computed when the vertically averaged circulation first reaches 20 $km^2 s^{-1}$, a value roughly midway through TD spinup and denoted by the horizontal dotted line in (a). The surface flux anomaly components in the control simulation are denoted by thin dashed curves in (b) and are not used to compute the ensemble mean.

prior to warm-core formation is consistent with Nolan (2007). Raymond and Sessions (2007) suggested that the stabilization of the troposphere, created by the warm over cold stratification associated with a midlevel vortex, aids in the creation of bottom-heavy convective mass flux profiles that are efficient in converging vorticity, which might suggest a propensity for midlevel vortex formation during TD spinup. However, there is disagreement in recent literature about Raymond and Sessions's (2007) finding (e.g., Lussier et al. 2013), and further investigation is required into the importance of midlevel vortices during TD spinup.

In all members of this ensemble, enhanced surface fluxes occur near the center of the vortex during TD spinup and are driven almost entirely by surface winds (Fig. 4b). Flux anomalies driven by air–sea enthalpy disequilibrium are weak in comparison, and consist of small, counteracting latent and sensible heat flux anomalies. In summary, the rate at which TD spinup occurs is only modestly sensitive to changes in CAPE and RH of the initial state, but somewhat more sensitive to the vertical structure of the seed vortex. In all cases, however, similar radial distributions of surface enthalpy fluxes occur during TD spinup and are driven almost exclusively by surface wind variations.

c. *Spinup driven by air–sea enthalpy disequilibrium*

While disequilibrium-driven surface fluxes played a negligible role during TD spinup in the control simulation, we now discuss a role for surface fluxes driven purely by the air–sea enthalpy disequilibrium. We conduct three simulations in which surface fluxes are prescribed to be independent of surface wind speed (Table 1, group C). TD spinup still occurs when the surface wind speeds are fixed at 10 $m s^{-1}$ in the surface flux parameterization (Mid5_Fix10), albeit more slowly than in the control, with a warm core forming on day 12 (compared to day 3 in the control; not shown). On day 10, peak winds occur at roughly 4-km altitude and at a radius of approximately 50 km (Fig. 5a). Compared to the TD in the control simulation, the vortex tilts radially outward.

Even though surface fluxes are prescribed to be independent of wind speed, spinup is still accompanied by enhanced surface fluxes near the vortex center (Fig. 5b, black curve). As in the control, the lower-tropospheric negative temperature anomalies associated with the midlevel vortex enhance the sensible heat flux (Fig. 5b, red curve). Additionally, the disequilibrium-driven surface evaporation is now positive and adds to, rather than opposes, the disequilibrium-driven sensible heat flux (Fig. 5b, blue curve). The fixed wind speed of 10 $m s^{-1}$ used in the surface flux parameterization enhances surface evaporation throughout the domain and maintains the boundary layer near saturation, depicted by an RH increase of approximately 10% below 500-m altitude at all radii (Fig. 5a). Bounded by its saturation value, the

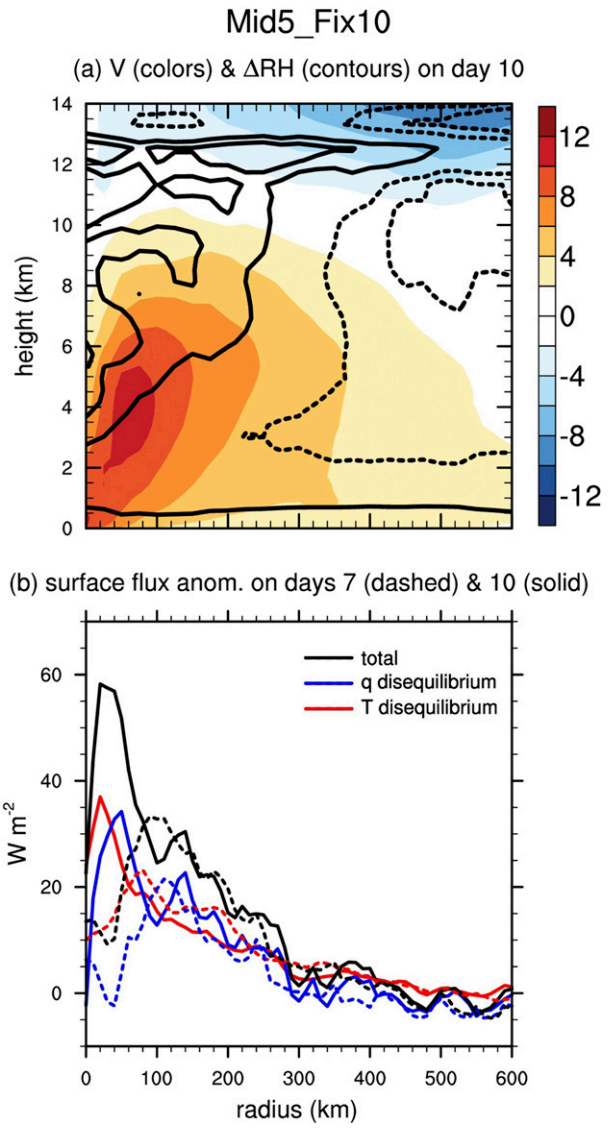

FIG. 5. As in Fig. 3, but for the simulation in which the surface wind is fixed at $10\,m\,s^{-1}$ in the surface flux parameterization (Mid5_Fix10). Note the smaller range of the horizontal axes compared to Fig. 3. Quantities on (a) day 10 and (b) days 7 (dashed) and 10 (solid). Wind-driven surface flux anomalies do not exist in this simulation and are not shown in (b).

surface air water vapor mixing ratio is thus lower in the cold core of the vortex than at large radii, leading to enhanced disequilibrium-driven surface evaporation in the vortex core. In contrast, the vortex core in the control simulation had higher specific humidity than its environment, due to the wind-enhanced surface evaporation, and so had reduced disequilibrium-driven surface evaporation in the vortex core. The existence of enhanced disequilibrium-driven evaporation thus seems to be a result of prescribing a relatively large wind speed in the surface flux formula, which brings the boundary layer near saturation and creates a positive radial gradient in the water vapor mixing ratio of surface air for a midlevel vortex. A negative radial gradient of surface enthalpy fluxes is thus obtained, driven purely by the enthalpy disequilibrium; this gradient is roughly a factor of 4 weaker than in the control simulation (peak surface fluxes of about $60\,W\,m^{-2}$ in Mid5_Fix10 compared to $250\,W\,m^{-2}$ in Mid5), consistent with the fact that it takes about 4 times as long for the warm core to form (the relationship between enthalpy flux gradients and intensification rates is quantified in section 6).

In this Mid5_Fix10 simulation, peak surface flux anomalies increase from roughly 35 to $60\,W\,m^{-2}$ between days 7 and 10 (Fig. 5b, dashed and solid black curves), accompanied by strengthening of the low-level cold core. In a separate simulation, we horizontally homogenize the air–sea enthalpy disequilibria [ΔT and Δq in Eq. (3)] in the surface flux formulas at each model time step, in addition to fixing surface wind speed. This eliminates the enhancement of surface fluxes near the vortex center and prevents TD spinup, implying that the feedback between the air–sea enthalpy disequilibrium of the vortex and the surface flux anomalies is essential for TD spinup when the wind speed is fixed in the surface flux formulas. Furthermore, capping the temperature and moisture disequilibrium at 5 K and $7\,g\,kg^{-1}$, respectively, reduces surface flux anomalies and slows TD spinup, with a warm core forming only after 18 days (not shown). Thus, while a continually increasing disequilibrium-driven feedback is not essential for intensification, intensification occurs more rapidly with this feedback.

Additionally, when surface fluxes are independent of wind speed, the disequilibrium-driven fluxes near the vortex center seem to increase with the wind speed prescribed in the surface flux parameterization and aid spinup. That is, changes in the enthalpy of surface air do not overcompensate for the imposed changes in wind speed in Eq. (3). When the surface wind is fixed at $5\,m\,s^{-1}$ in the surface flux parameterization (Mid5_Fix5), spinup proceeds more slowly than in Mid5_Fix10 and a warm-core vortex forms only on day 16 (not shown).

When initialized with a surface vortex and surface wind speeds are fixed at $10\,m\,s^{-1}$ in the surface flux parameterization (Sfc5_Fix10), TD spinup is initially suppressed owing to negative temperature and moisture disequilibria associated with the near-surface warm core. Intensification occurs after low-level divergence transforms the surface vortex into a midlevel vortex. The formation of the cold core enhances disequilibrium-driven sensible heat flux and surface evaporation during spinup, with a warm core forming on day 14 (not shown).

d. *Necessity of a negative radial gradient of surface fluxes*

Here, we examine whether the negative radial gradient of surface fluxes that has accompanied spinup in all prior simulations actually causes spinup by conducting a series of simulations in which horizontal inhomogeneities of surface fluxes are suppressed (Table 1, group D). As an extreme case, when surface enthalpy fluxes are entirely switched off, TD spinup fails to occur (Mid5_FlxOFF; Fig. 2c, red curve), consistent with Nguyen et al. (2008). This result might seem to differ from one of the findings of Montgomery et al. (2006), who find that a vortex can attain TD-strength surface winds without surface enthalpy fluxes. However, mean tangential surface winds intensified to only about 12 m s^{-1} in the first 24 h of their simulation, with no further intensification. Furthermore, Montgomery et al. (2006) initialized their model with a moister vortex, and we show in section 4g below that moister initial vortices also exhibit brief transient intensification in our model.

The necessity of surface flux feedback for intensification is also tested in a simulation in which the surface fluxes are fixed spatially and temporally. When surface evaporation is fixed at 200 W m^{-2} and sensible heat flux is switched off (Mid5_LHF200), the vortex fails to intensify (Fig. 6b, blue curve). Convective updrafts and downdrafts are distributed throughout the domain and the transverse secondary circulation fails to develop, despite any frictionally induced influence of the seed vortex. The fixed value of 200 W m^{-2} for latent heat flux is chosen to roughly match the peak surface fluxes in the control simulation (Fig. 3b). In additional simulations with surface enthalpy fluxes fixed at values between 50 and 350 W m^{-2}, the vortex also fails to intensify.

The failure of TD spinup to occur in the absence of a negative radial gradient of surface enthalpy fluxes is confirmed when surface enthalpy fluxes are horizontally homogenized at each model time step (Mid5_FlxHOM; Fig. 6b, red curve). These simulations support the hypothesis that surface enthalpy flux feedback, which manifests as a negative radial gradient of surface fluxes, are necessary for TD spinup, consistent with Montgomery et al. (2009).

e. *Role of surface evaporation*

The enhancement of surface enthalpy fluxes near the vortex center seems to be necessary for vortex intensification in our simulations, but how important is surface evaporation compared to surface sensible heat flux? Mrowiec et al. (2011) showed that TCs can intensify even in a dry axisymmetric model if the air–sea temperature disequilibrium is inflated to give the same net air–sea enthalpy disequilibrium as is typically observed over ocean.

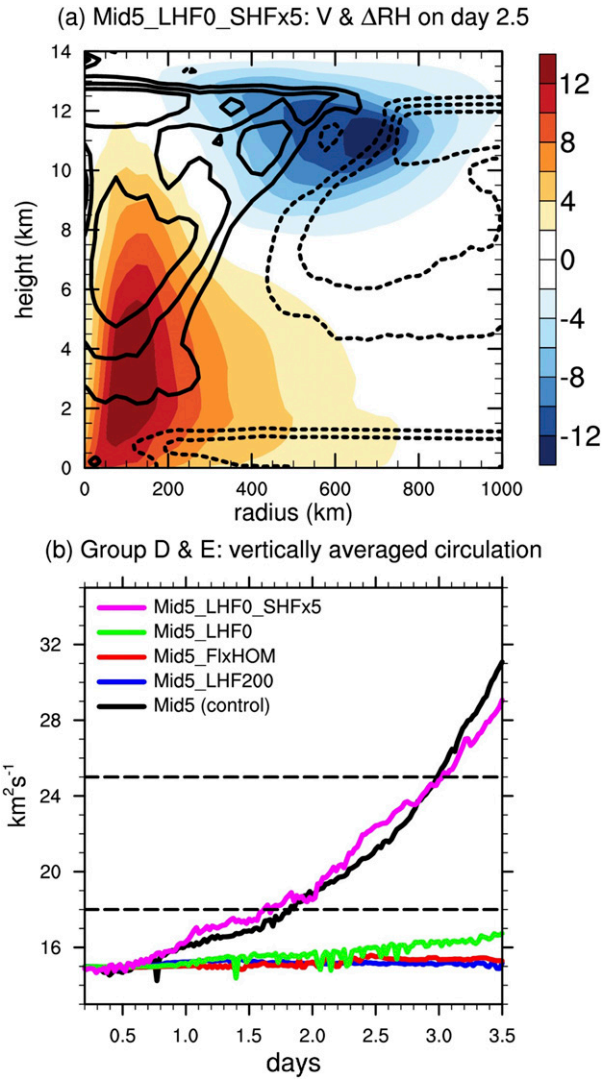

FIG. 6. (a) As in Fig. 3a, but for the simulation with latent heat fluxes switched off and sensible heat fluxes enhanced by a factor of 5 (Mid5_LHF0_SHFx5). (b) Time evolution of the 0–10-km vertically integrated circulation in a 500-km box tracking the vortex in a few selected group D and E simulations. Dashed lines in (b) indicate the lower (18 km^2 s^{-1}) and upper (25 km^2 s^{-1}) thresholds of circulation used to identify TDs.

So, is surface evaporation needed to moisten the initial vortex so that TC intensification can then proceed in a nearly saturated atmosphere, or would an equivalent amount of sensible heat flux produce a similar intensification?

Fritz and Wang (2014) and Kilroy et al. (2016) showed that, for an intensifying tropical storm, horizontal convergence of water vapor by the secondary circulation closely matched total precipitation and far exceeded surface evaporation. However, neither study compared surface evaporation with the Eulerian time tendency of precipitable water, here called water vapor storage,

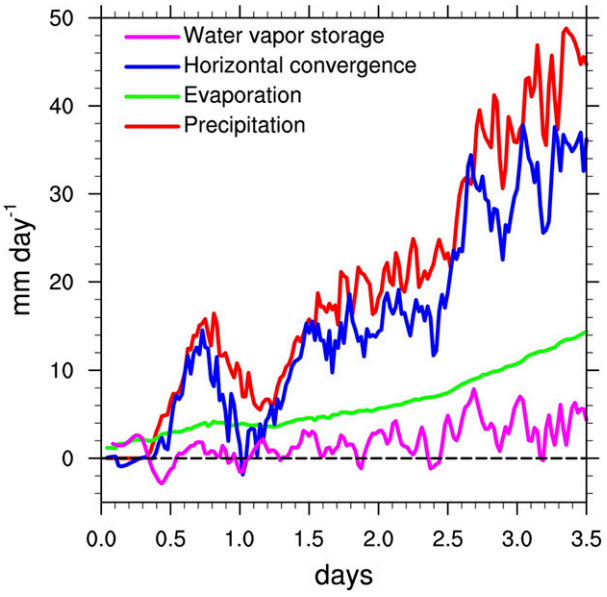

FIG. 7. Time evolution of the vertically integrated moisture budget terms in a 500-km box tracking the vortex in the control (Mid5) simulation.

during vortex moistening, although Kilroy et al. (2016) noted the lack of water budget closure in reanalyses. Closure of the vertically integrated water vapor budget in the idealized simulations of this study enables an accurate assessment of the role of surface evaporation as a moisture source during TD spinup.

The vertically integrated water vapor budget in our control simulation (Mid5) shows progressively larger values of precipitation over time nearly matched by the horizontal convergence of water vapor (Fig. 7), consistent with Fritz and Wang (2014) and Kilroy et al. (2016). However, surface evaporation is still larger than the storage term, even though it is small compared to horizontal convergence. Thus, based on diagnostics alone, one cannot eliminate the possibility that surface evaporation is needed to moisten the vortex and allow further intensification.

The simulations in group E are designed to clarify the role of surface evaporation in vortex intensification and moistening. In these simulations, surface latent heat flux is switched off and replaced by a roughly equivalent amount of sensible heat flux by multiplying the exchange coefficient for sensible heat flux C_H by 5 (Mid5_LHF0_SHFx5). The choice of this factor is guided by the average Bowen ratio in the control simulation, 0.25, which only marginally exceeds the composite-mean Bowen ratio observed in Atlantic hurricanes (0.2; Cione et al. 2000). This simulation may not have a physical analog in the real world but enables conclusions to be made about the role of surface evaporation in TD spinup.

In this simulation, TD spinup proceeds almost identically to the control (Fig. 6b, magenta curve). On day 2.5, midlevel cyclonic winds and RH are marginally greater than in the control simulation (Fig. 6a), and a warm core forms on day 3. The increase in moisture is driven only by the horizontal convergence of water vapor by the transverse secondary circulation, which exceeds precipitation (not shown). Since there is no moisture source in this simulation, vortex moistening is accompanied by drying in the lower and middle troposphere outside the vortex (Fig. 6a, dashed contours). While this does not impact the rate of TD spinup, intensification stops once the peak tangential surface wind speed reaches 56 m s^{-1} on day 7, compared to 87 m s^{-1} attained in the control simulation on day 8 (not shown). This extends the results of Mrowiec et al. (2011), who examined the simulated structure and evolution of TCs in the total absence of water, to a moist, precipitating vortex. The unaffected rate of TD spinup shows that the distinction between latent and sensible surface heat fluxes is not important in TD spinup, and it is the total surface enthalpy flux that maintains convective instability and precipitating ascent. Additionally, this result emphasizes the importance of water vapor convergence by the secondary circulation as the primary source of moisture during TD spinup, while underscoring the fact that this moisture convergence balances but does not cause precipitation.

We also conduct a simulation with surface evaporation switched off and interactive sensible heat fluxes, without any scaling of the transfer coefficient C_H. In this simulation (Mid5_LHF0), TD spinup is extremely slow (Fig. 6b, green curve). A warm-core vortex has not formed even after 10 days, but it is nevertheless notable that the vertically averaged circulation does increase over time, associated with weak ascent and a weak secondary circulation. Rapid spinup over ocean in our model thus requires either interactive surface evaporation or an inflated surface sensible heat flux.

f. Surface enthalpy fluxes with "capped" wind speeds

Montgomery et al. (2009) argued that TCs do not intensify through WISHE based in part on results from simulations in which the surface wind speed in the surface flux parameterization was limited to (i.e., capped at) modest values such as 7.5 or 10 m s^{-1}. However, Zhang and Emanuel (2016) showed that the observed intensification of at least one TC (Hurricane Edouard, 2014) could only be successfully simulated if surface fluxes were not limited in that fashion. The implication of these previous results for TD spinup is unclear, because surface wind speeds during TD intensification are often below the wind speed limits imposed by Montgomery et al. (2009).

Here we also conduct simulations with wind speeds capped in the surface flux formulas, but, unlike previous work, we focus on TD spinup and examine the radial distribution of surface enthalpy fluxes. Consistent with the relatively weak amplitude of TDs, we cap wind speeds in the surface flux formulas at 2 and 5 m s^{-1} in two separate simulations (Table 1, group F). Vortices in these simulations still intensify, but more slowly than in the control (Fig. 8a). There is still a clear negative radial gradient of surface enthalpy flux in both simulations, though it is also reduced in magnitude relative to that in the control (Fig. 8b; only wind-driven surface flux anomalies are plotted since the disequilibrium-driven anomalies are negligible). Even when surface winds are capped at the small value of 2 m s^{-1}, surface fluxes are enhanced by approximately 80 W m^{-2} at the radius of maximum wind compared to the vortex periphery, which remains very quiescent; intensification is so slow in this case that a warm-core vortex has not formed even after 10 days, but the vertically averaged circulation does still increase over time.

These results show that, while a continual increase of surface fluxes with surface winds is not required to achieve TD spinup, the fastest rates of intensification are only possible if this feedback is not inhibited, consistent with Zhang and Emanuel (2016). Furthermore, the rate of intensification here increases with the magnitude of surface flux anomalies near the vortex center, challenging the interpretation of the role of surface fluxes presented by Montgomery et al. (2009).

g. *Transient intensification of nearly saturated vortices*

Our last set of simulations examines the evolution of extremely moist initial conditions, motivated by previous studies in which a moist vortex was simulated as reaching intensities characteristic of TDs without surface flux feedback. In particular, Montgomery et al. (2006) stated that mean near-surface tangential winds of about 12 m s^{-1} were achieved 24 h after initialization of their model, even though surface enthalpy fluxes were turned off, but that no further intensification occurred. Does this disprove the conclusion suggested by all of our other simulations and show that surface enthalpy flux feedback is not needed to maintain convective instability and precipitating ascent during TD spinup?

We initialize these simulations (Table 1, group G) by imposing a nearly saturated region (RH up to 95%) of 300-km radius in the center of the domain. The axisymmetric moisture anomaly used in these simulations is almost entirely confined to the free troposphere (Fig. 1b, contours), and its details are given in the appendix. When this humidity field is imposed with our standard midlevel vortex as an initial condition, intensification is rapid and tropical storm intensity is attained within the first day (Mid5_Moist; Fig. 9, orange curve). This demonstrates the importance of moistening in TD spinup: much of the roughly 3-day-long spinup process in the control simulation seems to be needed primarily for

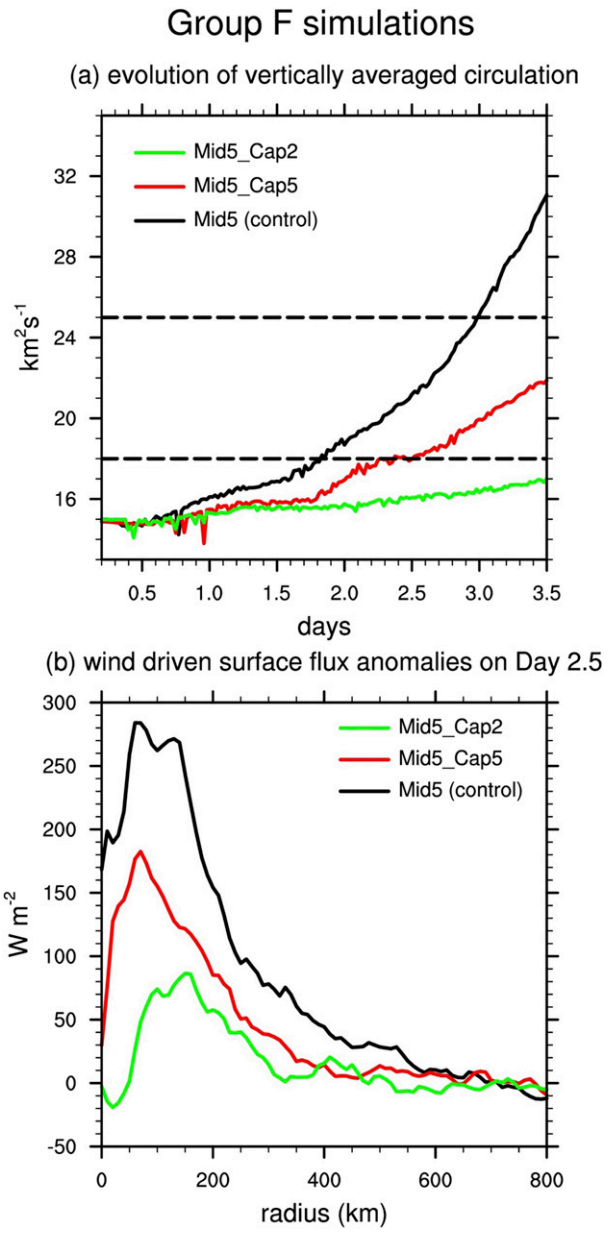

FIG. 8. (a) Evolution of the vertically averaged circulation and (b) wind-driven surface flux anomalies on day 2.5 for simulations of group F, wherein surface wind speeds are capped in the surface flux parameterization. Surface flux anomalies are calculated with respect to the domain mean. Dashed lines in (a) indicate the lower (18 km^2 s^{-1}) and upper (25 km^2 s^{-1}) thresholds of circulation used to identify TDs.

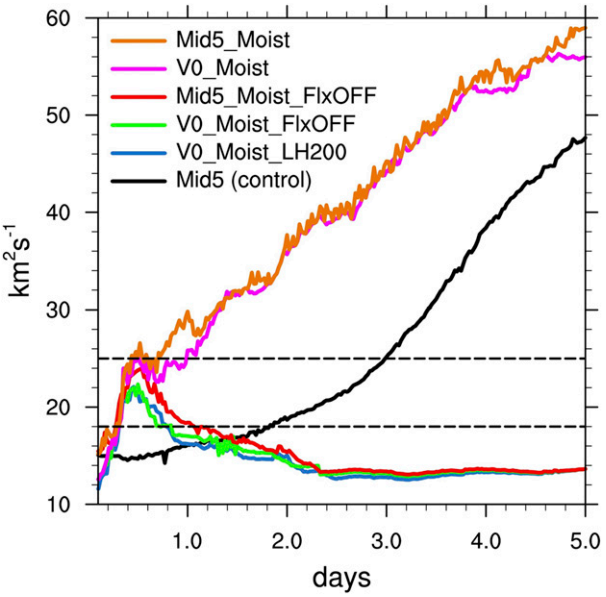

FIG. 9. Time evolution of the 0–10-km vertically integrated circulation in a 500-km box tracking the vortex in simulations initialized with an axisymmetric moist anomaly (group G). Dashed lines indicate the lower ($18\,km^2\,s^{-1}$) and upper ($25\,km^2\,s^{-1}$) thresholds of circulation used to identify TDs. The circulation associated with the control simulation (Mid5; black curve) is plotted for reference.

tropospheric moistening, because that spinup process is shortened dramatically when a very moist initial condition is used. A nearly saturated vortex facilitates convective updrafts from the onset of the simulation and accelerates spinup. Although our initial moisture anomaly is accompanied by positive virtual temperature anomalies, those anomalies peak at 0.21 K at about 6-km altitude and are only about 20% as large as the peak warm anomalies in our midlevel and surface vortices, which intensify more slowly (e.g., cf. Figs. 9 and 4a). The moist anomaly thus seems to produce faster intensification through its effect on precipitating convection rather than through its virtual temperature effect on the rotational dynamics.

More remarkable is the result that nearly identical rapid intensification can be achieved using the humidity anomaly alone without a seed vortex (i.e., by initializing the model to a state of rest with the same axisymmetric moisture anomaly just discussed). The magenta curve in Fig. 9 shows the intensification for this simulation (V0_Moist). The most rapid spinup in all of our simulations thus occurs for an axisymmetric moisture anomaly, regardless of whether an initial vortex is imposed. The rotational dynamics thus respond quite rapidly to the influence of an axisymmetric free-tropospheric moisture anomaly on the distribution of convection, more so than they do to changes in the vertical structure of the seed vortex or even to the entire elimination of the seed vortex.

A very moist seed vortex is able to undergo TD spinup when surface enthalpy fluxes are completely turned off (Mid5_Moist_FlxOFF), consistent with the result of Montgomery et al. (2006). TD spinup is rapid, with vertically averaged circulation of approximately $24\,km^2\,s^{-1}$ and peak near-surface tangential wind of $11\,m\,s^{-1}$ achieved after 12 h (Fig. 9, red curve). The ambient convective instability in the initial condition, along with high column relative humidity values near the vortex center, results in precipitating ascent and convergence of vorticity and moisture. However, this spinup is transient and not sustained, indicated by the reduction in circulation to less than its initial value by day 3.

A nearly saturated moisture anomaly at a state of rest undergoes similar transient intensification (V0_Moist_FlxOFF; Fig. 9, green curve). In this simulation, a TD-strength vortex forms within 12 h, with peak tangential winds of $13\,m\,s^{-1}$ at roughly 4-km altitude confined to radii where RH exceeds 90% (Fig. 10a). However, in the absence of surface fluxes, a warm-core vortex fails to form and the vortex and its associated moisture dissipate rapidly. After 5 days, only a weak vortex with peak wind speeds of $6\,m\,s^{-1}$ and no associated moisture remains (Fig. 10b). This shows that the moisture converged by the secondary circulation in the boundary layer does not increase convective instability and support the sustained precipitating ascent required for TD spinup and that enhanced surface enthalpy fluxes near the vortex center are required.

Similar transient intensification is seen when a moist anomaly is allowed to evolve from rest with surface evaporation fixed at a horizontally uniform value of $200\,W\,m^{-2}$ (V0_Moist_LH200; Fig. 9, blue curve). This confirms that, even for a very moist initial vortex, it is not the amplitude of the domain-mean surface enthalpy flux that matters but the enthalpy flux feedback with the vortex state. Additionally, while the horizontal convergence of moisture far exceeds surface evaporation and is the primary source of moisture during TD spinup, moisture convergence does not increase convective instability; convective instability near the vortex center is instead generated primarily by surface enthalpy fluxes.

5. Quantifying the rate of TD spinup

The role of enhanced surface flux in TD spinup is quantitatively assessed across all of our simulations using the framework developed by R07, after some modification. This framework relates the rate of change of the vertically averaged circulation Γ to surface fluxes of enthalpy and momentum in a nascent TD. Here we

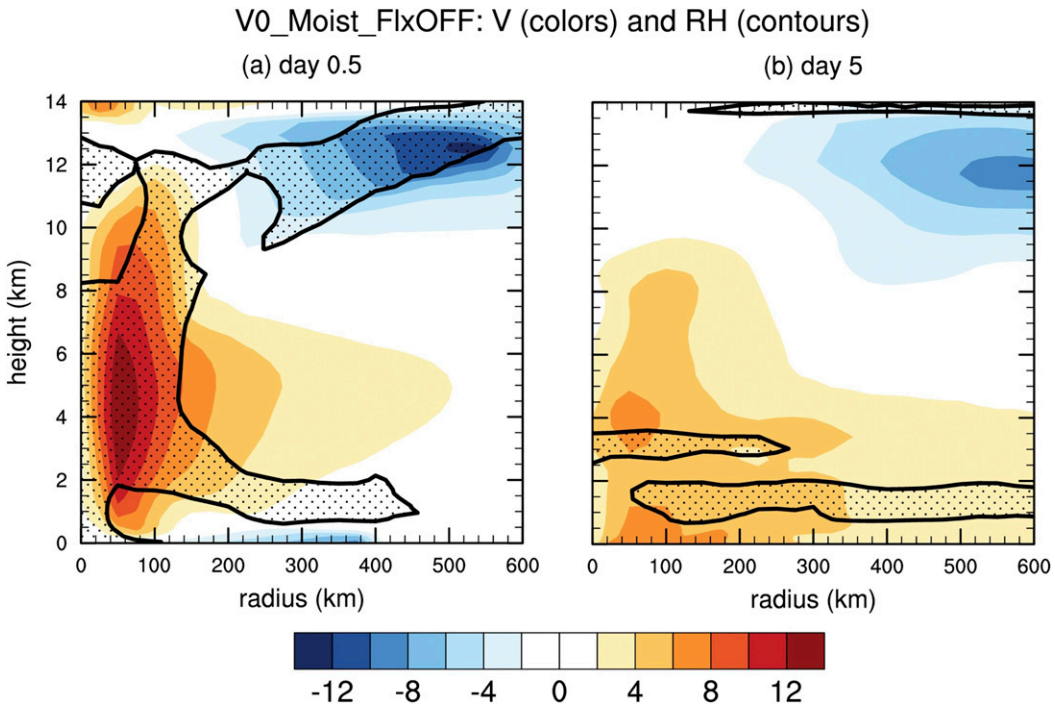

FIG. 10. Azimuthal-average tangential winds (colors) and RH (contours; stippling indicates RH > 90%) on (a) day 0.5 and (b) day 5 in the simulation initialized with no tangential winds, an axisymmetric moist anomaly, and surface fluxes switched off (V0_Moist_FlxOFF).

present the framework and its underlying assumptions and then use it to diagnose the rate of TD spinup in our simulations.

First, the vorticity equation is integrated horizontally and averaged vertically over the same domain used in Eq. (2) and temporally averaged over the duration of TD spinup (which lasts at least 3 days in our simulations):

$$\left[\frac{\partial \Gamma}{\partial t}\right] = -\left[\iint \langle \nabla \cdot (\mathbf{u}\zeta_a)\rangle \, dx\, dy\right] - \left[\iint \langle \nabla \cdot (\mathbf{k} \times \mathbf{F})\rangle \, dx\, dy\right], \tag{4}$$

where ζ_a is absolute vorticity, $\mathbf{F}$ represents horizontal viscous and turbulent forces, and the square brackets denote temporal averages during TD spinup. Like R07, we omit the "tilting" term, $\omega \partial_p \mathbf{u}$, by neglecting the vertical velocity ω on the periphery of the area of integration, consistent with the dominant role of the advective vorticity flux (Wang 2012).

We now seek to relate the convergence of vorticity to surface enthalpy fluxes using the gross moist stability (GMS; Neelin and Held 1987), which in turn relates large-scale ascent to column-integrated energy sources. If vertical structures of humidity and wind change in time, the GMS will also change and thus will not provide a useful constraint for relating convergence to surface fluxes; it may thus seem unwise to use the GMS in a theory for an intensifying, precipitating vortex. However, we assume here that variations in the GMS are sufficiently small on time scales of several days or longer. This assumption is consistent with the convective quasi-equilibrium hypothesis (CQE; Arakawa and Schubert 1974; Emanuel et al. 1994), in which convection eliminates variations in CAPE on time scales longer than those of the individual convective elements over which it averages. Models based on CQE can be used to constrain the GMS (Raymond et al. 2009). Storm-scale ascent and circulation can vary greatly even when column-integrated energy sources are fixed, but in our simulations such variations occurred on shorter time scales of a day or less (e.g., the V0_Moist runs in Fig. 9).

While numerical models based on CQE have successfully simulated TCs (Emanuel 2007) and increases of both boundary layer and upper-tropospheric equivalent potential temperature have been seen during TC intensification in idealized cloud-system-resolving simulations (Miyamoto and Takemi 2013), a more thorough examination of the validity of CQE during TD spinup has not been performed. Nie et al. (2010) found that CQE is valid in the seasonal mean in multiple monsoon regions (e.g., South Asia, Australia, and South Africa)

but is not valid to the same extent in others (e.g., South America and North America), perhaps as a result of topography, intrusions of dry midtropospheric air, large-scale influences from midlatitude systems, and remote effects from other monsoon systems. None of these factors exist in our idealized simulations, but the applicability of CQE to diagnose TD spinup remains unclear and is thus further examined here.

Using the same diagnostic as Nie et al. (2010), the boundary layer equivalent potential temperature θ_{eb} (vertically averaged between the surface and 1 km) and upper-level saturation equivalent potential temperature θ_e^* (vertically averaged between 6 and 12 km) are compared in all our simulations. Both quantities are horizontally averaged in the 500-km box surrounding the vortex center, and temporally averaged during TD spinup, similar to the averaging regions in Eq. (4). Figure 11 shows that θ_{eb} and θ_e^* are highly correlated in all of our simulations, implying that CQE holds in the horizontal and temporal domains chosen in our quantitative framework. To be clear, we conclude only that CQE can be used to describe the system-scale evolution of a TD-like vortex in our idealized model on time scales of 2–3 days or longer. We expect CQE to break down on shorter time and space scales, and also to be less valid as unbalanced, boundary layer dynamics become more important as the system intensifies into a tropical storm or hurricane.

The GMS is given by

$$\gamma \equiv \frac{[\mathrm{SF} - R]}{[\{\nabla \cdot \mathbf{u}\}_-]}, \tag{5}$$

with R the column-integrated radiative flux divergence, $\{\nabla \cdot \mathbf{u}\}_-$ the vertical integral of the negative part of the divergence profile, computed between the surface and 10 km, and the curly braces denoting the vertical integral between the surface and 10 km. For simplicity, we deviate from R07 here and do not normalize the GMS by the moisture flux convergence nor weight our vertical average of the vorticity equation by the mixing ratio. Furthermore, Eq. (5) is derived from the energy budget rather than the entropy budget, so its numerator does not contain the irreversible production term that appears (but was subsequently neglected) in the moist entropy budget used in R07.

For a weak vortex in an environment of negligible horizontal shear, the advective vorticity flux can be approximated by the convergence of planetary vorticity [i.e., $\nabla \cdot (\mathbf{u}\zeta_a) \simeq f\nabla \cdot \mathbf{u}$]. This approximation is valid in our simulations during the early stages of TD spinup examined here, but invalid during subsequent stages of intensification (not shown), consistent with Tory and

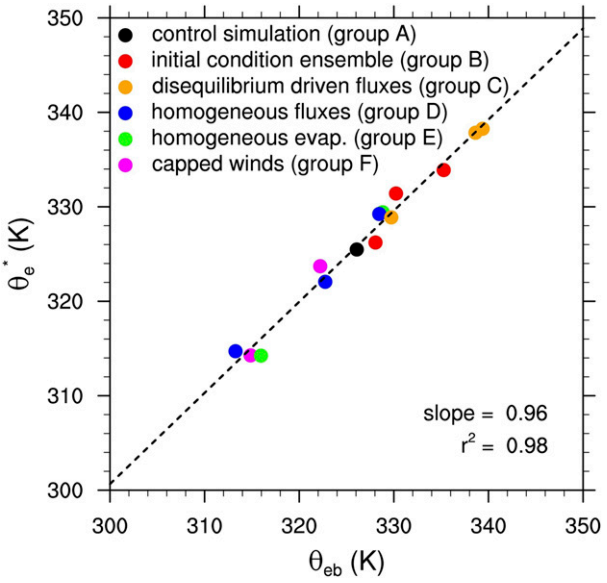

FIG. 11. Boundary layer equivalent potential temperature θ_{eb} and upper-level saturation equivalent potential temperature θ_e^* in all our simulations (except group G). Both quantities have been horizontally averaged in a 500-km box surrounding the vortex center and temporally averaged during TD spinup.

Montgomery (2008). Using Eq. (5) to represent the vertical integral of mass convergence in Eq. (4) yields

$$\left[\frac{\partial \Gamma}{\partial t}\right] = \frac{1}{\gamma}\left(\frac{f}{M}\iint [\mathrm{SF} - R]\,dx\,dy\right) + \frac{1}{M}\iint [\nabla \cdot (\mathbf{k} \times \mathbf{T})]\,dx\,dy, \tag{6}$$

where the surface drag $\mathbf{T}$ is the mass-weighted vertical integral of the frictional force $\mathbf{F}$, and M is the vertically integrated mass of the initial sounding.

Finally, we neglect the modification of R by the vortex (i.e., $R = \overline{R}$) and equate the domain-mean vertically integrated radiative flux divergence $\overline{R}$ and surface enthalpy fluxes $\overline{\mathrm{SF}}$, which is essentially the RCE approximation. Hence, Eq. (6) becomes

$$\left[\frac{\partial \Gamma}{\partial t}\right] = \frac{1}{\gamma}\left(\frac{f}{M}\iint [\mathrm{SF}']\,dx\,dy\right) + \frac{1}{M}\iint [\nabla \cdot (\mathbf{k} \times \mathbf{T})]\,dx\,dy. \tag{7}$$

The first term on the right-hand side represents the spinup tendency due to vorticity convergence by the large-scale ascent needed to export the column energy input by anomalous surface fluxes, while the second term represents the damping effects of drag. Because of the underlying assumptions and the presence of horizontally and temporally averaged terms, Eq. (7) can

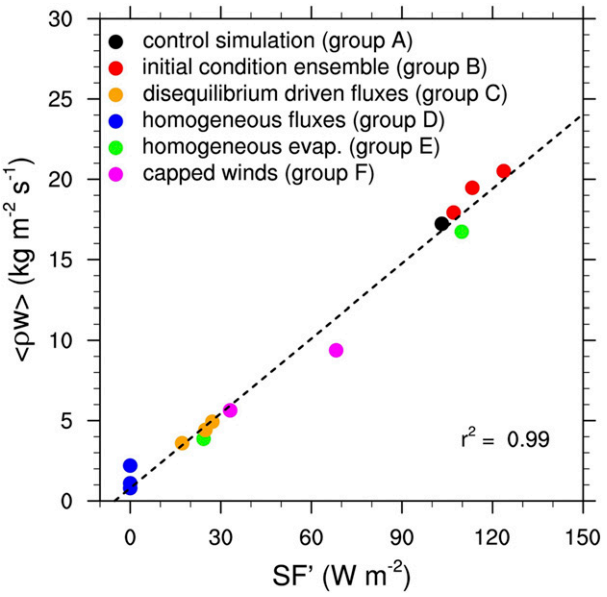

FIG. 12. Surface flux anomalies with respect to the domain-mean SF′ and vertically averaged vertical mass flux $\langle \rho w \rangle$ in all our simulations (except group G). Both quantities have been horizontally averaged in a 500-km box surrounding the vortex center and temporally averaged during TD spinup. Prime quantities indicate departures from the domain mean and angle brackets indicate mass-weighted vertical averages.

only be used to diagnose system-scale TD spinup on multiday time scales.

We now briefly examine one of the central assumptions in the formulation of the first term on the right-hand side of Eq. (7): Do variations in ascent scale linearly with variations in surface enthalpy flux, as implied by Eq. (5) with a constant GMS? Figure 12 shows the relation between vertical mass flux horizontally averaged near the vortex center and the surface enthalpy flux anomaly averaged over that same region. Other proxies for the strength of precipitating ascent, such as precipitation and horizontal mass convergence, display a similar pattern, with higher values seen for more positive surface flux anomalies. Thus, when the surface flux anomalies are allowed to become larger and are not inhibited in our idealized simulations, the precipitating ascent is stronger and is associated with a greater convergence of vorticity. Note that while a statistical association does not generally imply causation, in some of our simulations the surface flux distribution was imposed (e.g., group D), so it is clear that in those simulations the circulation anomalies did not cause the surface flux anomalies.

The spindown tendency due to drag, the second term on the right-hand side of Eq. (7), is equal to the line integral of surface drag on the periphery of our domain, which under a bulk flux formula is $-4a\rho_0 C_D U^2/M$ for a square domain of width a and drag coefficient C_D. Using Eq. (1) to represent SF′ with $C_E = C_H = C_D$, we can estimate the relative magnitude of the spinup and spindown tendencies (i.e., the ratio of the first and the second terms) as

$$\frac{af\Delta k}{4\gamma U}, \tag{8}$$

with Δk the air–sea enthalpy disequilibrium. For $U = 10\,\mathrm{m\,s^{-1}}$ and $\Delta k = 20\,\mathrm{kJ\,kg^{-1}}$, this ratio is between 25 and 2.5 for values of γ between 500 (e.g., Yu et al. 1998) and $5000\,\mathrm{J\,kg^{-1}}$ (e.g., R07, their normalized GMS of 0.5 converted using a $5\,\mathrm{g\,kg^{-1}}$ difference between moisture in the inflow and outflow layers). In any case, the spindown tendency given by the line integral of the drag is smaller than that estimated by R07 for TDs with radii less than 500 km. The above treatment assumes drag to be distributed over the full depth of the vortex, perhaps by convective momentum transports and the continual readjustment of the vortex toward gradient wind balance, whereas R07 assumed drag confined to the surface layer but discussed the possibility that it might have a larger vertical length scale. In our control simulation and in Sfc5 (the initial vortex expected to exhibit the strongest drag), the spindown tendency in Eq. (7) due to surface friction is about 1/15 the circulation tendency when it is calculated to apply between the surface and 10 km. This may explain why our seed vortices intensify even though they have radii well below the critical radius of 1600 km predicted by R07 to be necessary for intensification.

Since the spindown term due to drag seems to be small, we compare $\partial_t \Gamma$ and the spinup term in each of our simulations, with each term averaged between the start of the simulation and the time at which Γ reaches $25\,\mathrm{km^2\,s^{-1}}$ (in simulations without spinup, averages are computed up to day 5). The intensification rate is well correlated with the spinup term (Fig. 13). The spinup term, which depends only on surface flux anomalies in this framework, is a function of the vortex state via its surface wind speed or air–sea enthalpy disequilibrium; if surface fluxes increase linearly with the circulation, the first two terms in Eq. (7) describe a positive feedback between surface fluxes and circulation. Even though the drag spindown term may not be negligible, the relationship shown in Fig. 13 indicates that it is smaller than the spinup term in Eq. (7) and that a linear scaling approximates the relationship between the bulk radial gradient of surface enthalpy fluxes and the vortex intensification rate in this ensemble of idealized simulations.

We emphasize that Eq. (7) provides no description of the dynamics of TD spinup. It is based on the assumption that the column-integrated energy source scales

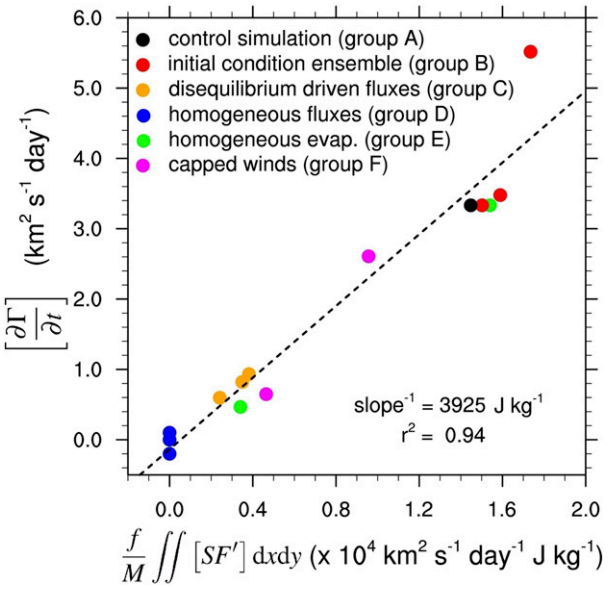

FIG. 13. Time tendency of vertically averaged circulation on the y axis compared with the term inside the parentheses in the spinup tendency in Eq. (7) on the x axis in all our simulations (except group G).

linearly with storm-scale ascent, as in R07, and is only intended to approximate the system-scale intensification of a TD over time scales of a few days or longer. Transient intensification on shorter time scales does occur in our simulations initialized with a very moist vortex and without interactive surface fluxes (e.g., group G and Fig. 9), and we speculate that this transient intensification is associated with the release of CAPE (or entraining CAPE) on time scales shorter than those on which a convective quasi-equilibrium hypothesis would apply and on which the GMS would remain roughly constant. These simulations exhibiting transient spinup are not plotted in Fig. 13.

6. Summary and discussion

Surface flux feedback during TD spinup is examined here using idealized, three-dimensional, cloud-system-resolving simulations of intensifying vortices over uniform SST. All simulations support the hypothesis that a negative radial gradient of surface enthalpy flux, with enhanced surface flux near the vortex center, is required for TD spinup. In contrast, Montgomery et al. (2015, p. 92) stated that, for TC intensification to occur, "some minimal enthalpy fluxes are only needed to maintain convection"; our results directly refute the idea that, for TD spinup, spatial and temporal variations in surface enthalpy flux are not required as long as that flux exceeds some minimal value.

By decomposing the surface flux into wind- and enthalpy-disequilibrium-driven components, we show that TD spinup occurs most rapidly when surface enthalpy flux is enhanced by surface winds, with the disequilibrium-driven feedback being comparatively weak. TD spinup occurs and is accompanied by a negative radial gradient of surface enthalpy flux even when surface fluxes are prescribed to be independent of surface winds, owing to a negative radial gradient of air–sea enthalpy disequilibrium. In this case, however, TD spinup occurs slowly and at a rate dependent on the uniform wind speed imposed in the surface flux parameterization. Spinup fails to occur when surface flux feedback is switched off and surface fluxes are horizontally homogeneous. TD spinup is severely limited when the feedback is reduced by limiting (i.e., capping) the wind speed in the surface flux formulas.

Additionally, when surface evaporation is replaced by a roughly equivalent amount of sensible heat flux, vortex intensification and moistening is nearly identical to the control simulation. This result shows that the distinction between latent and sensible heat fluxes is unimportant during spinup and that it is the total surface enthalpy flux that matters, at least in this idealized model. This extends the results of Mrowiec et al. (2011) to a framework with explicit precipitation and encourages further examination of observed genesis and spinup of depression-like cyclonic vortices over land (e.g., Hurley and Boos 2015), where surface evaporation is limited but where abundant moisture could be fluxed from nearby oceans.

From a thermodynamic perspective, intensification and moistening of a TD is associated with an increase in its moist entropy, which can be achieved via multiple pathways: import by the secondary circulation, enhanced surface enthalpy fluxes, or reduced radiative cooling. The reciprocal of the slope of the best-fit line in Fig. 13 suggests a positive GMS value across our simulations and thus an export of moist entropy by the secondary circulation. We also found (although it was not a main focus) that spinup still occurred when radiative temperature tendencies were horizontally homogenized at each model time step. Nevertheless, our analyses did not focus on the transport of moist entropy by the secondary circulation or on the role of interactions between radiation, water vapor, and clouds; further investigation of these processes during TD spinup is thus needed.

Finally, we showed that a moist vortex undergoes TD spinup in the absence of surface flux feedback, but only in a transient, brief, and unsustained manner, lasting less than 24 h. Surface flux feedback continued to be necessary for sustained intensification of a moist vortex and

subsequent transition to a warm-core vortex. This result complements previous emphasis on the negative radial gradient of column relative humidity during TC intensification (e.g., Emanuel 1997; Frisius 2006). While a negative radial gradient of surface enthalpy fluxes, which fosters greater convective instability near the vortex center, is one pathway to achieve a persistent saturated column with sustained convection, other pathways could potentially exist. However, large-scale horizontal convergence of moisture alone does not enhance convective instability or cause precipitation; horizontal moisture convergence is indeed the primary moisture source that balances the precipitation sink during TD spinup, but radial inflow cannot increase the amplitude of the maximum in a conserved variable such as θ_{eb}.

The negative radial gradient of surface fluxes required for TD spinup was generated by two primary mechanisms in the idealized simulations used in this study. In a quiescent environment (e.g., simulations in groups A and B in Table 1), surface fluxes were enhanced by surface winds. Alternatively, when sufficiently strong uniform surface winds were imposed in the bulk flux formulas, which might be taken to represent a gusty environment, the air–sea thermodynamic disequilibrium enhanced the surface fluxes and led to spinup, albeit more slowly. Whether some part of the spinup process in observed TDs might be caused by air–sea thermodynamic disequilibrium is unclear, but further investigation seems merited given that typical trade wind speeds of roughly $5\,\mathrm{m\,s^{-1}}$ are comparable to azimuthal surface wind speeds in the initial stages of spinup. Further investigation of the role of surface flux feedback mechanisms in more realistic background states would help in understanding such issues.

Finally, strong vertical wind shear is generally detrimental to TC genesis owing to the import of lower-entropy dry air that inhibits deep convection (Simpson and Riehl 1958). Yet weak wind shear can also accelerate TC genesis by forcing large-scale ascent (e.g., Nolan and McGauley 2012). While most TCs experience some degree of vertical wind shear, the vortices in our simulations are allowed to intensify in its absence. The importance of surface enthalpy fluxes for TD spinup in the presence of vertical wind shear merits examination in future work.

Acknowledgments. This work was supported by Office of Naval Research Awards N00014-11-1-0617 and N00014-15-1-2531 and by the Yale Center for Research Computing. We thank Zhuo Wang and two anonymous reviewers for comments that improved the manuscript.

APPENDIX

Initialization of the Seed Vortex and Moisture Anomaly

a. Seed vortex

Here, we describe the structure of the seed vortex in our simulations. The temperature perturbation is considered first, followed by the balance used to compute tangential winds.

The axisymmetric temperature perturbation $T'(r, z)$ is the product of separate vertical (T'_z) and radial (T'_r) structures. The vertical structure is governed by the maximum negative anomaly ($T'_- = -2.5\,\mathrm{K}$), the maximum positive anomaly ($T'_+ = 1.05\,\mathrm{K}$), the height of maximum winds ($z_m = 3\,\mathrm{km}$), and the vertical extent of the vortex ($z_t = 11\,\mathrm{km}$):

$$T'_z(z) = \begin{cases} T'_- \exp\left(-\dfrac{z^2}{z_m^2/8}\right), & \text{for} \quad z \le z_m \\ T'_+ \exp\left[-\dfrac{(z - z_{\mathrm{mid}})^2}{(z_t - z_m)^2/32}\right], & \text{for} \quad z > z_m \end{cases}, \tag{A1}$$

where $z_{\mathrm{mid}} = (z_m + z_t)/2$. The radial structure is governed by the radius at which the tangential winds vanish ($r_{\mathrm{end}} = 500\,\mathrm{km}$), given by

$$T'_r(r) = \exp\left(-\frac{r^2}{r_{\mathrm{end}}^2/8}\right). \tag{A2}$$

The resulting temperature anomaly for the control simulation is shown in Fig. 1a (contours).

The axisymmetric pressure p and density ρ are computed using the hydrostatic approximation and ideal gas law:

$$\frac{\partial p}{\partial z} = -\rho g, \qquad \rho = \frac{p}{R_d T(1 + 0.61q)}, \tag{A3}$$

where T is the total temperature (including the anomaly T'), q is the water vapor mixing ratio from the sounding, R_d is the gas constant for dry air ($287\,\mathrm{J\,kg^{-1}\,K^{-1}}$), and g is the gravitational acceleration. The hydrostatic equation is integrated from the top of the model to the surface, with ρ calculated using the ideal gas law at each height. Pressure and density at the top level are obtained from the initial sounding.

Gradient wind balance in cylindrical coordinates is

$$\frac{v^2}{r} + fv = \frac{1}{\rho}\frac{\partial p}{\partial r}, \tag{A4}$$

with v the tangential wind. The balanced tangential wind at each height is obtained from the vertical derivative of gradient wind balance:

$$\frac{\partial v}{\partial z} = -\frac{1}{\rho}\frac{\frac{1}{\rho}\frac{\partial p}{\partial r}\frac{\partial \rho}{\partial z} + g\frac{\partial \rho}{\partial r}}{\frac{2v}{r} + f}. \tag{A5}$$

This Eq. (A5) is integrated downward from $v = 0$ at the top of the model to obtain the axisymmetric tangential winds as a function of r and z. Centered finite-difference schemes are used to compute the radial and vertical derivatives in Eq. (A5), except at the boundaries where appropriate forward or backward difference schemes are used. Tangential winds in the control simulation are plotted in Fig. 1a (colors).

b. Moisture anomaly

The axisymmetric, positive RH anomaly introduced into the center of the domain in a few simulations (Table 1, group G) is the product of separate vertical (RH'_z) and radial (RH'_r) functions. The vertical structure is specified in terms of its maximum value ($\mathrm{RH}'_{\max} = 30\%$) and its bottom ($z_b = 1$ km) and top ($z_t = 11$ km) boundaries:

$$\mathrm{RH}'_z(z) = \mathrm{RH}'_{\max}\exp\left[-\frac{(z - z_{\mathrm{mid}})^2}{(z_t - z_b)^2/32}\right], \tag{A6}$$

where $z_{\mathrm{mid}} = (z_b + z_t)/2$. The RH anomaly peaks at the center of the domain and vanishes at radius $r_{\mathrm{end}} = 300$ km with a radial distribution

$$\mathrm{RH}'_r(r) = \exp\left(-\frac{r^2}{r_{\mathrm{end}}^2/8}\right). \tag{A7}$$

The RH anomaly is shown in Fig. 1b (contours). The total RH is not allowed to exceed a maximum value of 95%.

REFERENCES

Arakawa, A., and W. H. Schubert, 1974: Interaction of a cumulus cloud ensemble with the large-scale environment, Part I. *J. Atmos. Sci.*, **31**, 674–701, https://doi.org/10.1175/1520-0469(1974)031<0674:IOACCE>2.0.CO;2.

Bister, M., and K. A. Emanuel, 1997: The genesis of Hurricane Guillermo: TEXMEX analyses and a modeling study. *Mon. Wea. Rev.*, **125**, 2662–2682, https://doi.org/10.1175/1520-0493(1997)125<2662:TGOHGT>2.0.CO;2.

Cione, J. J., P. G. Black, and S. H. Houston, 2000: Surface observations in the hurricane environment. *Mon. Wea. Rev.*, **128**, 1550–1561, https://doi.org/10.1175/1520-0493(2000)128<1550:SOITHE>2.0.CO;2.

Cohen, N. Y., and W. R. Boos, 2016: Perspectives on moist baroclinic instability: Implications for the growth of monsoon depressions. *J. Atmos. Sci.*, **73**, 1767–1788, https://doi.org/10.1175/JAS-D-15-0254.1.

Davis, C. A., and L. F. Bosart, 2003: Baroclinically induced tropical cyclogenesis. *Mon. Wea. Rev.*, **131**, 2730–2747, https://doi.org/10.1175/1520-0493(2003)131<2730:BITC>2.0.CO;2.

——, and D. A. Ahijevych, 2013: Thermodynamic environments of deep convection in Atlantic tropical disturbances. *J. Atmos. Sci.*, **70**, 1912–1928, https://doi.org/10.1175/JAS-D-12-0278.1.

Ditchek, S. D., W. R. Boos, S. J. Camargo, and M. K. Tippett, 2016: A genesis index for monsoon disturbances. *J. Climate*, **29**, 5189–5203, https://doi.org/10.1175/JCLI-D-15-0704.1.

Dunkerton, T. J., M. T. Montgomery, and Z. Wang, 2009: Tropical cyclogenesis in a tropical wave critical layer: Easterly waves. *Atmos. Chem. Phys.*, **9**, 5587–5646, https://doi.org/10.5194/acp-9-5587-2009.

Emanuel, K. A., 1986: An air-sea interaction theory for tropical cyclones. Part I: Steady-state maintenance. *J. Atmos. Sci.*, **43**, 585–605, https://doi.org/10.1175/1520-0469(1986)043<0585:AASITF>2.0.CO;2.

——, 1989: The finite-amplitude nature of tropical cyclogenesis. *J. Atmos. Sci.*, **46**, 3431–3456, https://doi.org/10.1175/1520-0469(1989)046<3431:TFANOT>2.0.CO;2.

——, 1997: Some aspects of hurricane inner-core dynamics and energetics. *J. Atmos. Sci.*, **54**, 1014–1026, https://doi.org/10.1175/1520-0469(1997)054<1014:SAOHIC>2.0.CO;2.

——, 2003: Tropical cyclones. *Annu. Rev. Earth Planet. Sci.*, **31**, 75–104, https://doi.org/10.1146/annurev.earth.31.100901.141259.

——, 2007: Quasi-equilibrium dynamics of the tropical atmosphere. *The Global Circulation of the Atmosphere*, T. Schneider and A. Sobel, Eds., Princeton University Press, 186–218.

——, J. D. Neelin, and C. S. Bretherton, 1994: On large-scale circulations in convecting atmospheres. *Quart. J. Roy. Meteor. Soc.*, **120**, 1111–1143, https://doi.org/10.1002/qj.49712051902.

Frisius, T., 2006: Surface-flux-induced tropical cyclogenesis within an axisymmetric atmospheric balanced model. *Quart. J. Roy. Meteor. Soc.*, **132**, 2603–2623, https://doi.org/10.1256/qj.06.03.

Fritz, C., and Z. Wang, 2014: Water vapor budget in a developing tropical cyclone and its implication for tropical cyclone formation. *J. Atmos. Sci.*, **71**, 4321–4332, https://doi.org/10.1175/JAS-D-13-0378.1.

Hendricks, E. A., M. T. Montgomery, and C. A. Davis, 2004: The role of "vortical" hot towers in the formation of Tropical Cyclone Diana (1984). *J. Atmos. Sci.*, **61**, 1209–1232, https://doi.org/10.1175/1520-0469(2004)061<1209:TROVHT>2.0.CO;2.

Hurley, J. V., and W. R. Boos, 2015: A global climatology of monsoon low-pressure systems. *Quart. J. Roy. Meteor. Soc.*, **141**, 1049–1064, https://doi.org/10.1002/qj.2447.

Khairoutdinov, M. F., and K. Emanuel, 2013: Rotating radiative-convective equilibrium simulated by a cloud-resolving model. *J. Adv. Model. Earth Syst.*, **5**, 816–825, https://doi.org/10.1002/2013MS000253.

——, and D. A. Randall, 2003: Cloud resolving modeling of the ARM summer 1997 IOP: Model formulation, results, uncertainties, and sensitivities. *J. Atmos. Sci.*, **60**, 607–625, https://doi.org/10.1175/1520-0469(2003)060<0607:CRMOTA>2.0.CO;2.

Kiehl, J. T., J. J. Hack, G. B. Bonan, B. A. Boville, D. L. Williamson, and P. J. Rasch, 1998: The National Center for Atmospheric Research Community Climate Model: CCM3. *J. Climate*, **11**, 1131–1149, https://doi.org/10.1175/1520-0442(1998)011<1131:TNCFAR>2.0.CO;2.

Kilroy, G., R. K. Smith, M. T. Montgomery, B. Lynch, and C. Earl-Spurr, 2016: A case-study of a monsoon low that formed over the

sea and intensified over land as seen in ECMWF analyses. *Quart. J. Roy. Meteor. Soc.*, **142**, 2244–2255, https://doi.org/10.1002/qj.2814.

——, ——, and ——, 2017: A unified view of tropical cyclogenesis and intensification. *Quart. J. Roy. Meteor. Soc.*, **143**, 450–462, https://doi.org/10.1002/qj.2934.

Lussier, L. L., M. T. Montgomery, and M. M. Bell, 2013: The genesis of Typhoon Nuri as observed during the tropical cyclone structure 2008 (TCS-08) field experiment—Part 3: Dynamics of low-level spin-up during the genesis. *Atmos. Chem. Phys.*, **14**, 8795–8812, https://doi.org/10.5194/acpd-13-26795-2013.

Marín, J. C., D. J. Raymond, and G. B. Raga, 2008: Intensification of tropical cyclones in the GFS model. *Atmos. Chem. Phys.*, **9**, 1407–1417, https://doi.org/10.5194/acpd-8-17803-2008.

Miyamoto, Y., and T. Takemi, 2013: A transition mechanism for the spontaneous axisymmetric intensification of tropical cyclones. *J. Atmos. Sci.*, **70**, 112–129, https://doi.org/10.1175/JAS-D-11-0285.1.

Molinari, J., D. Vollaro, and K. L. Corbosiero, 2004: Tropical cyclone formation in a sheared environment: A case study. *J. Atmos. Sci.*, **61**, 2493–2509, https://doi.org/10.1175/JAS3291.1.

Montgomery, M. T., and R. K. Smith, 2017: Recent developments in the fluid dynamics of tropical cyclones. *Annu. Rev. Fluid Mech.*, **49**, 541–574, https://doi.org/10.1146/annurev-fluid-010816-060022.

——, M. E. Nicholls, T. A. Cram, and A. B. Saunders, 2006: A vortical hot tower route to tropical cyclogenesis. *J. Atmos. Sci.*, **63**, 355–386, https://doi.org/10.1175/JAS3604.1.

——, N. V. Sang, R. K. Smith, and J. Persing, 2009: Do tropical cyclones intensify by WISHE? *Quart. J. Roy. Meteor. Soc.*, **135**, 1697–1714, https://doi.org/10.1002/qj.459.

——, J. Persing, and R. K. Smith, 2015: Putting to rest WISHE-ful misconceptions for tropical cyclone intensification. *J. Adv. Model. Earth Syst.*, **7**, 92–109, https://doi.org/10.1002/2014MS000362.

Mrowiec, A. A., S. T. Garner, and O. M. Pauluis, 2011: Axisymmetric hurricane in a dry atmosphere: Theoretical framework and numerical experiments. *J. Atmos. Sci.*, **68**, 1607–1619, https://doi.org/10.1175/2011JAS3639.1.

Neelin, J. D., and I. M. Held, 1987: Modeling tropical convergence based on the moist static energy budget. *Mon. Wea. Rev.*, **115**, 3–12, https://doi.org/10.1175/1520-0493(1987)115<0003:MTCBOT>2.0.CO;2.

Nguyen, V. S., R. K. Smith, and M. T. Montgomery, 2008: Tropical-cyclone intensification and predictability in three dimensions. *Quart. J. Roy. Meteor. Soc.*, **134**, 563–582, https://doi.org/10.1002/qj.235.

Nie, J., W. R. Boos, and Z. Kuang, 2010: Observational evaluation of a convective quasi-equilibrium view of monsoons. *J. Climate*, **23**, 4416–4428, https://doi.org/10.1175/2010JCLI3505.1.

Nolan, D. S., 2007: What is the trigger for tropical cyclogenesis. *Aust. Meteor. Mag.*, **56**, 241–266.

——, and M. G. McGauley, 2012: Tropical cyclogenesis in wind shear: Climatological relationships and physical processes. *Cyclones: Formation, Triggers and Control*, K. Oouchi and H. Fudeyasu, Eds., Nova Science Publishers, 1–36.

——, E. D. Rappin, and K. A. Emanuel, 2007: Tropical cyclogenesis sensitivity to environmental parameters in radiative-convective equilibrium. *Quart. J. Roy. Meteor. Soc.*, **133**, 2085–2107, https://doi.org/10.1002/qj.170.

Palmen, E., 1948: On the formation and structure of tropical hurricanes. *Geophysica*, **3**, 26–38.

Raymond, D. J., 2012: Balanced thermal structure of an intensifying tropical cyclone. *Tellus*, **64A**,

——, and S. L. Sessions, 2007: Evolution of convection during tropical cyclogenesis. *Geophys. Res. Lett.*, **34**, L06811, https://doi.org/10.1029/2006GL028607.

——, and C. López-Carrillo, 2011: The vorticity budget of developing Typhoon Nuri (2008). *Atmos. Chem. Phys.*, **11**, 147–163, https://doi.org/10.5194/acp-11-147-2011.

——, ——, and L. L. Cavazos, 1998: Case-studies of developing east Pacific easterly waves. *Quart. J. Roy. Meteor. Soc.*, **124**, 2005–2034, https://doi.org/10.1002/qj.49712455011.

——, S. L. Sessions, and Ž. Fuchs, 2007: A theory for the spinup of tropical depressions. *Quart. J. Roy. Meteor. Soc.*, **133**, 1743–1754, https://doi.org/10.1002/qj.125.

——, ——, A. H. Sobel, and Ž. Fuchs, 2009: The mechanics of gross moist stability. *J. Adv. Model Earth Syst.*, **1** (9), https://doi.org/10.3894/JAMES.2009.1.9.

Romps, D. M., 2014: An analytical model for tropical relative humidity. *J. Climate*, **27**, 7432–7449, https://doi.org/10.1175/JCLI-D-14-00255.1.

Rotunno, R., and K. A. Emanuel, 1987: An air–sea interaction theory for tropical cyclones. Part II: Evolutionary study using a nonhydrostatic axisymmetric numerical model. *J. Atmos. Sci.*, **44**, 542–561, https://doi.org/10.1175/1520-0469(1987)044<0542:AAITFT>2.0.CO;2.

Saha, K., F. Sanders, and J. Shukla, 1981: Westward propagating predecessors of monsoon depressions. *Mon. Wea. Rev.*, **109**, 330–343, https://doi.org/10.1175/1520-0493(1981)109<0330:WPPOMD>2.0.CO;2.

Simpson, R., and H. Riehl, 1958: Mid-tropospheric ventilation as a constraint on hurricane development and maintenance. Preprints, *10th Conf. on Hurricanes*, Miami Beach, FL, Amer. Meteor. Soc., D4.1–D4.10.

Tang, B. H., 2017: Coupled dynamic–thermodynamic forcings during tropical cyclogenesis. Part I: Diagnostic framework. *J. Atmos. Sci.*, **74**, 2269–2278, https://doi.org/10.1175/JAS-D-17-0048.1.

Tory, K. J., and M. Montgomery, 2008: Tropical cyclone formation: A synopsis of the internal dynamics. *28th Conf. on Hurricanes and Tropical Meteorology*, Orlando, FL, Amer. Meteor. Soc., 10A.1, https://ams.confex.com/ams/28Hurricanes/techprogram/paper_138062.htm.

——, and W. M. Frank, 2010: Tropical cyclone formation. *Global Perspectives on Tropical Cyclones: From Science to Mitigation*, J. Chan and J. Kepert, Eds., World Scientific, 55–91.

Wang, Z., 2012: Thermodynamic aspects of tropical cyclone formation. *J. Atmos. Sci.*, **69**, 2433–2451, https://doi.org/10.1175/JAS-D-11-0298.1.

——, 2014: Role of cumulus congestus in tropical cyclone formation in a high-resolution numerical model simulation. *J. Atmos. Sci.*, **71**, 1681–1700, https://doi.org/10.1175/JAS-D-13-0257.1.

Wing, A. A., and K. A. Emanuel, 2014: Physical mechanisms controlling self-aggregation of convection in idealized numerical modeling simulations. *J. Adv. Model. Earth Syst.*, **6**, 59–74, https://doi.org/10.1002/2013MS000269.

——, S. J. Camargo, and A. H. Sobel, 2016: Role of radiative–convective feedbacks in spontaneous tropical cyclogenesis in idealized numerical simulations. *J. Atmos. Sci.*, **73**, 2633–2642, https://doi.org/10.1175/JAS-D-15-0380.1.

Yanai, M., 1961: A detailed analysis of typhoon formation. *J. Meteor. Soc. Japan*, **39**, 187–214, https://doi.org/10.2151/jmsj1923.39.4_187.

Yu, J.-Y., C. Chou, and J. D. Neelin, 1998: Estimating the gross moist stability of the tropical atmosphere. *J. Atmos. Sci.*, **55**, 1354–1372, https://doi.org/10.1175/1520-0469(1998)055<1354:ETGMSO>2.0.CO;2.

Zhang, F., and K. Emanuel, 2016: On the role of surface fluxes and WISHE in tropical cyclone intensification. *J. Atmos. Sci.*, **73**, 2011–2019, https://doi.org/10.1175/JAS-D-16-0011.1.